Zeitschrift für Angewandte
Mathematik und Mechanik

WILEY-VCH

Application of the One-Dimensional Turbulence model to incompressible channel and pipe flow

Journal:	*Zeitschrift für Angewandte Mathematik und Mechanik*
Manuscript ID	Draft
Wiley - Manuscript type:	Original Paper
Date Submitted by the Author:	n/a
Complete List of Authors:	Medina Méndez, Juan; Brandenburgische Technische Universitat Cottbus-Senftenberg, Numerische Strömungs- und Gasdynamik Schmidt, Heiko; Brandenburgische Technische Universität Cottbus-Senftenberg, Numerische Strömungs- und Gasdynamik Lignell, David; Brigham Young University
Keywords:	ODT, channel, pipe, temporal, spatial

SCHOLARONE™
Manuscripts

ORIGINAL PAPER

Application of the One-Dimensional Turbulence model to incompressible channel and pipe flow

Juan A. Medina Méndez*[1] | Heiko Schmidt[1] | David O. Lignell[2]

[1]Chair of Numerical Fluid and Gas
Dynamics, Brandenburg University of
Technology (BTU) Cottbus-Senftenberg,
Brandenburg, Germany
[2]Chemical Engineering Department,
Brigham Young University, Utah, USA

Correspondence
*Corresponding author. Email:
medinjua@b-tu.de

Present Address
Siemens-Halske-Ring 14, LG3A R160,
03046 Cottbus, Germany.

Summary

Incompressible channel and pipe flow configurations are investigated using the One-Dimensional Turbulence (ODT) model, in which the 1-D domain is aligned with the wall normal direction. A framework for the application of ODT in planar and cylindrical coordinates is revisited for temporal ODT channel and pipe flow configurations, and a new spatial formulation is introduced. The calculation of the turbulent kinetic energy (TKE) budgets in ODT for the temporal and spatial formulations is reviewed for the planar channel flow, and newly introduced in cylindrical pipe flow. Simulations are performed at three different friction Reynolds numbers, 550, 1000 and 2000, in order to compare ODT results for velocity statistics in the planar and cylindrical formulation with Direct Numerical Simulations (DNS) from Chin et al. [Int. J. Heat Fluid Flow 45 (2014) 33-40] and Khoury et al. [Flow, Turbul. Comb. 91 (2013) 475-495]. The efficiency of the model for simulating lower Reynolds number flows is also evaluated with comparison of ODT results for velocity and passive temperature statistics to the DNS data from Satake and Kunugi [Int. J. Numer. Methods Heat Fluid Flow 12(8) (2002) 958-1008]. The results show that a representative part of the first and second order statistical moments for pipe and channel flows can be captured in a satisfactory way with ODT. For applications in the studied Reynolds number range, ODT is a highly appealing complementary tool to DNS.

KEYWORDS:
ODT, channel, pipe, temporal, spatial

1 | INTRODUCTION

Although the canonical channel and pipe flow configurations have been studied extensively, there are still numerous issues in the field of wall-bounded flows that have not been properly addressed. A very detailed list of issues and the current state of the art is presented by Marusic et al.[1]. Open discussions in wall-bounded flows focus on the structure and scaling of wall turbulence at high Reynolds numbers. On one hand, there is the classical scaling approach, directly related to the mean velocity behavior and the two principal regions of the velocity profile that follow distinct scalings. On the other hand, there is the more complex topic of observation of coherent organized motions and their effect on turbulent interactions, e.g. in turbulence production[1].

A comprehensive study on the mean velocity characteristics in turbulent pipe flow is given by Wu and Moin[2]. That study presents a solid discussion from the classical scaling point of view by means of Direct Numerical Simulations (DNS), for a range of bulk Reynolds numbers $5300 < Re_D < 44000$. Monty et al.[3] provide a detailed introduction to the topic, experimental

results of the large-scale structures away from the wall, and how they are more likely to grow at a greater rate with distance from the wall in channels. Also adding to this point is the discussion presented by Kim and Adrian[4], regarding the existence of very large-scale motions (VLSMs), prominent in the logarithmic layer of turbulent pipe flow.

Significant contributions that could help ellucidate the open questions in wall-bounded flows could, and should be eventually addressed by DNS. However, while DNS have pushed the limits of current computational power, only modest Reynolds numbers up to $Re_\tau = 3008$ have been achieved for pipe flow[5]. The simplicity of the channel flow configuration allowed the achievement of these moderately high Reynolds numbers earlier[6,7]. There is an important lag between DNS studies and experimental turbulence measurements, given that the latest experimental studies have been able to achieve Re_τ up to 98000[8].

Turbulence models such as the Reynolds-Averaged Navier-Stokes (RANS) or Large Eddy Simulations (LES) are computationally less expensive in comparison to DNS. These are ideally applicable, however, when there is a clear separation of scales in the flow dynamics and the small or non-resolved scales can be modelled[9]. Problems aimed at addressing fundamental questions, such as the turbulence scaling itself and the turbulence dynamics characterization cannot be solved by the former turbulence models given that the behavior of the small scales is not always understood. PDF transport methods are an alternative in this case, however, their main limitation resides on the choice of suitable mixing models[10]. Recently, a new branch of statistical modeling based on the benefits of machine learning has been introduced. Wu et al.[11] propose a novel approach for a RANS closure method involving a machine learning algorithm from DNS training sets is described and validated. The cases studied by Wu et al.[11] are carefully selected in a way that shows the features of the algorithm; these are cases where RANS models would have severe performance limitations (cases involving secondary flow and separation events). Ma et al.[12,13] also applied Neural Networks (NN) for the generation of RANS closure terms. As with any machine learning approach, the limitation of the suggested algorithms resides in the availability of training sets, in this case, the availability of DNS studies that need to be used as an input for the learning algorithm.

In contrast to RANS, LES, or traditional PDF transport methods, i.e., instead of modeling length-scales or molecular mixing/diffusion processes, Kerstein developed the One-Dimensional Turbulence model (ODT)[14]. In ODT, all molecular diffusion is resolved directly, as in DNS, but only in 1-D. 3-D turbulence is modelled by means of a solution-dependent sequence of stochastic 1-D eddy events. For turbulent boundary layer-type problems, ODT is a cost-effective model that can complement DNS, and which may provide insights, although with less fidelity, at parameter ranges that are not accessible to DNS. So far, ODT has been validated in a variety of flows (see e.g.[15,16,17,18,19,20,21]). In this study, we focus on a new cylindrical formulation for incompressible pipe flow in ODT, as a way to extend the model into more complex flows. The cylindrical formulation for ODT was first introduced by Krishnamoorthy[18]. Lignell et al. recently developed a more comprehensive framework for the cylindrical formulation[22]. In the present work, we expand the latter formulation with a spatial formulation for closed systems in the radial direction, and introduce the ODT turbulent kinetic energy (TKE) equations in the cylindrical case, along with calculation examples for production and dissipation budgets.

This paper is structured as follows: Section 2 provides the model details for the simulation of incompressible channel and pipe flow. We begin with a brief overview of the fundamentals behind the stochastic part implementation in ODT, relying heavily on the work of Lignell et al.[22] for general aspects of the cylindrical formulation, and focusing the analysis on the limitations encountered by the formulation in radially closed systems. Afterwards, we discuss the derivation of the diffusion equations in ODT for the temporal formulation, and we then generalize some concepts for a new spatial formulation in radially closed systems. Section 3 details the derivation of relevant statistical quantities in ODT, with the purpose of deriving and introducing the cylindrical ODT turbulent kinetic energy (TKE) equation. Section 4 discusses the application of the model for velocity statistics in moderate and large Reynolds number regimes, comparing ODT results to DNS data[23,6,7,24,25,26]. Section 5 discusses the application of the model for lower Reynolds number regimes, comparing ODT velocity and passive scalar temperature statistics with DNS data[24,27]. Finally, some concluding remarks are provided in Section 6.

2 | ODT MODEL FORMULATION FOR INCOMPRESSIBLE CHANNEL AND PIPE FLOW

In the ODT model, the deterministic solution of 1-D diffusion (and possible reaction) evolution equations is coupled to the stochastic implementation of 1-D eddy events. An eddy event in ODT models the effects of turbulent transport due to eddies on the 1-D property profiles of the flow. Concurrently, the deterministic diffusion process catches up to implemented eddy events, in what could be considered as a two-step operator splitting approach. Following this categorization, details of the eddy event
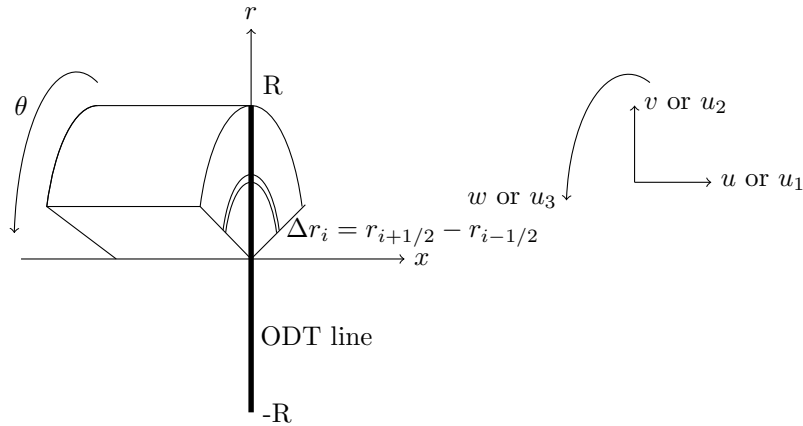
FIGURE 1 Representation of an ODT line in a cylindrical coordinate system. An exemplary cell with size Δr_i is shown to illustrate the form of the effective area/volume element of the cell, i.e. a ring element.

implementation are given in Section 2.1, while the form and derivation of the 1-D deterministic diffusion equations is described in Section 2.2.

2.1 | Stochastic turbulent advection

The stochastic turbulent advection process in ODT has been extensively detailed in previous publications. A complete discussion regarding the eddy event implementation is given by Lignell et al.[16,22] for the planar and cylindrical ODT formulations, respectively. In this section, we just discuss some fundamental aspects of the stochastic turbulent advection treatment and the limitations of the model regarding the spatial formulation in channel and pipe flows.

The implementation of an eddy event is characterized by the application of the triplet map to the 1-D scalar profiles governing the flow conditions[14]. Operationally, the planar triplet map is defined as a threefold spatial reduction or compression of a given property profile within some specific eddy range $[y_0, y_0 + l]$, where y_0 is the left edge of the eddy and l is the length of the eddy, or eddy size. This compressed profile is then copied three times along the eddy range with the middle copy spatially inverted. This procedure conserves all quantities within the eddy range and introduces no discontinuities in the function[14]. A derivation of the transformation function describing the cylindrical triplet map can be found in APPENDIX A.

ODT can be used with a single velocity component, or in a vector formulation, in which three velocity components are modelled. The latter is facilitated with a so-called kernel function that is added to velocity components after mapping to effect inter-component energy transfer in a way that conserves both momentum and energy. In the case of the single velocity component treatment, the measure preserving property of the triplet map guarantees kinetic energy conservation[14]. This is because the line integral of u^2 would be conserved before and after mapping. Generally, however, it is desired to model the 3-D dynamics with ODT, and therefore many studies rely on the implementation of the previously mentioned kernel function[16,20,21]. For the planar ODT vector formulation, the velocity mapping follows the work from Ashurst and Kerstein[28],

$$u_k(y) \rightarrow u_k[f(y)] + c_k K(y) + b_k J(y). \tag{1}$$

Here, $K(y)$, $J(y)$ are kernel functions, while c_k and b_k are the respective kernel function coefficients, as defined by Ashurst and Kerstein[28] for the planar ODT formulation ($k \in \{1, 2, 3\}$). $f(y)$ is the triplet map transformation[28].

We now specialize the analysis to the cylindrical formulation. In the case of pipe flows, the planar philosophy is maintained concerning the application of two kernel functions to the mapped velocity field, as in Eq. (1), but substituting y by r. The velocity field notation u_k and the cylindrical system configuration follows in this case the nomenclature given in Figure 1 . Also, $f(y)$ is changed to $f(r)$, whereby $f(r)$ refers to the transformation rule given in the cylindrical case by Eq. (A9). As in the planar case, the kernel functions K, J are defined as

$$K(r) = r - f(r), \quad J(r) = |K(r)|. \tag{2}$$

In general, as in previous publications, there are three main parameters governing the implementation of an eddy event: r_0, l and λ. r_0 refers to the eddy position, specifically the position of the left edge of the eddy. l is the eddy size as before. λ is an

eddy rate distribution governing the sampling and selection of eddies,

$$\lambda = \frac{C}{l^2 \xi}. \tag{3}$$

Here, C is an ODT model parameter governing the frequency of events, or the magnitude of the eddy rate. The eddy rate λ is directly related to the ODT formulation used. As detailed in Lignell et al.[16,22], a temporal ODT formulation (T-ODT) considers a temporally developing line through the turbulent flow, while a spatial (S-ODT) formulation describes the stationary streamwise parabolic flow of individual fluid parcels which are advected with their local streamwise velocity. In both formulations, the direction of the ODT line coincides with the direction of dominant transport. For channel and pipe flows, this direction is the cross-wise or radial direction, respectively. In T-ODT, ξ is identically equal to a modelled eddy turnover time τ (the unit of ξ or τ is s), while in S-ODT, it is equal to a modelled characteristic streamwise eddy length scale (the unit of ξ is m). Whether it is interpreted as a time or a length scale, ξ can be calculated for a given eddy on the basis of the kinetic energy (T-ODT) or kinetic energy flux (S-ODT) implied during the corresponding eddy event,

$$E'_{kin,T-ODT} \sim \frac{1}{2} \left(\frac{\int_{r_0}^{r_0+l} \rho[f(r)]K^2 r dr}{\xi^2} \right), \quad \text{or} \quad E'_{kin,S-ODT} \sim \frac{1}{2} \widetilde{u}_1^2[f(r)] \left(\frac{\int_{r_0}^{r_0+l} \rho[f(r)]u_1[f(r)]K^2 r dr}{\xi^2} \right). \tag{4}$$

E'_{kin} in T-ODT is interpreted as a kinetic energy per unit area in the planar formulation, and a kinetic energy per unit length in the cylindrical formulation. In S-ODT, E'_{kin} is a kinetic energy flux per unit area in the planar formulation, and a flux per unit length in the cylindrical formulation. $\widetilde{u}_1$ is a bulk average of the streamwise velocity in the interval $[r_0, r_0+l]$. The integrals in Eq. (4) are evaluated with r_0 and l sampled from a presumed Probability Density Function (PDF) for eddy sizes and locations $\widehat{P}(r_0, l)$[16]. We define $E'_{kin} = E_{kin} - Z E_{vp}$ as the remaining kinetic energy after the subtraction of an energetic viscous penalty E_{vp} from the available kinetic energy (or kinetic energy flux) E_{kin}. Z is an ODT model parameter, i.e., a non dimensional scaling factor for the magnitude of E_{vp}. This energetic viscous penalty forbids implementation of very small eddies, which would otherwise be instantly dissipated as heat[28]. Additionally, for wall-bounded flows, Z acts as a tuning parameter for 3-D buffer layer dynamics which can not be captured by ODT[14,19]. A detailed procedure and all of the equations for the calculation of E_{kin}, E_{vp}, the kernel coefficients c_k and b_k in Eq. (1), as well as the exact (equality) definition of Eq. (4), can be found in Lignell et al.[16,22].

The evaluation of ξ, and subsequently of λ by Eq. (3) allows the calculation of a probability P defined by the ratio between the potential outcome λ and all possible potential eddies denoted by the global rate $\Lambda = \int \int \lambda dr_0 dl$. The calculation of Λ is too expensive in terms of computational cost, and therefore, an approximation of the acceptance probability of the eddy, P_a, is estimated on the basis of the thinning and rejection methods[16,22]. In the thinning method, eddies are sampled in time (or streamwise direction) as a Poisson process. In the rejection method, eddies are accepted based on the ratio between the unknown P and $\widehat{P}$. The product from the acceptance probabilities by the thinning and rejection methods, $P_a = P_{a,t}P_{a,r}$, leads to[16,22],

$$P_{a,T-ODT} = \frac{\lambda(r_0, l, t)\Delta t_{sampling}}{\widehat{P}(r_0, l)} \quad \text{or} \quad P_{a,S-ODT} = \frac{\lambda(r_0, l, x)\Delta x_{sampling}}{\widehat{P}(r_0, l)}. \tag{5}$$

Algorithmically, the calculated P_a of every candidate eddy leads to the decision of acceptance or rejection of the eddy. $\Delta t_{sampling}$ (or $\Delta x_{sampling}$) are variable sampling time (or streamwise) intervals, which are adjusted dynamically during the simulation, in order to ensure that $P_a < 1$[16,22].

We note that due to the sampling from $\widehat{P}$, the eddy selection algorithm may ocassionally implement unphysically large eddies[14]. As in Schmidt et al.[19], we address this topic from the physical point of view of restricting the places where eddies can occur by their maximum length-scale L_{max}. This is based on the assumption of the limitation of the turbulent stirring due to the walls. By restricting the eddy event size by construction, the Large-Eddy-Suppression mechanism typically done in ODT formulations can be avoided for wall-bounded flows such as channel or pipe flows[19]. Unlike C or Z, L_{max} is normally not considered a model parameter in the ODT literature and is generally not subject to detailed sensitivity studies. This is because L_{max} values are effectively bounded between 0 and the ODT domain length. Furthermore, very small values of L_{max} may result in the complete suppression of turbulent transport in limited wall-bounded flow, due to the small eddy counterpart suppression by the Z parameter. Due to this reason, the range of values for L_{max} is very reduced in comparison to C or Z.

Finally, we discuss now an important limitation of the model regarding the application of the S-ODT formulation for channel and pipe flows. We note that momentum conservation before and after the eddy event in the T-ODT formulation implies,

$$\int_{r_0}^{r_0+l} \rho[f(r)] \left\{ u_k[f(r)] + c_k K(r) + b_k J(r) \right\} r dr = \int_{r_0}^{r_0+l} \rho[f(r)]u_k[f(r)] r dr. \tag{6}$$

The reader should note that, strictly speaking, the RHS of Eq. (6) shows the mapped profiles $\rho[f(r)]$ and $u_k[f(r)]$ instead of the original profiles $\rho(r)$ and $u_k(r)$, due to the necessary condition for mass conservation in the line during an eddy event. Mass conservation is obtained by the measure preserving property of the triplet map transformation while mapping the density $\int \rho(r)r\mathrm{d}r = \int \rho[f(r)]r\mathrm{d}r$. Since the transformation rule is applied simultaneously to all of the flow variables, the starting point for the discussion of the energy redistribution procedure due to the implementation of the kernel functions must consider the post-mapped scalar profiles. This is analogous in S-ODT. For S-ODT in cylindrical pipe flow, the resulting momentum conservation gives,

$$\int_{r_0}^{r_0+l} \rho[f(r)]u_1[f(r)] \left\{ u_k[f(r)] + c_k K(r) + b_k J(r) \right\} r\mathrm{d}r = \int_{r_0}^{r_0+l} \rho[f(r)]u_1[f(r)]u_k[f(r)]r\mathrm{d}r. \tag{7}$$

The appearance of u_1 arises from the net streamwise momentum flux in the spatial formulation. As explained by Krishnamoorthy[18] for the cylindrical formulation, and by Ashurst and Kerstein[28] for the planar formulation, Eq. (7) is not internally consistent, since the factor $u_1[f(r)]$ is multiplied both in the LHS (at the end of the eddy event) and RHS (after/before triplet mapping). Instead of the fully mapped and kernel-transformed function on the LHS, only the mapped function appears. This is normally not a problem, since the traditional spatial formulation considers one additional step for the eddy implementation, in which the discretized cell boundaries are moved to new lateral locations in order to conserve streamwise fluxes[28]. That is, a coordinate transformation $r \rightarrow \hat{r}$ takes place after mapping, such that

$$\int_{-R}^{R} \rho[f(r)] \left\{ u_1[f(r)] + c_1 K(r) + b_1 J(r) \right\} \hat{r}\mathrm{d}\hat{r} = \int_{-R}^{R} \rho[f(r)]u_1[f(r)]r\mathrm{d}r. \tag{8}$$

Eq. (8) is the solution for streamwise momentum conservation based on lateral displacements along the entire computational domain, from $-R$ to R. We note that the identity $r\mathrm{d}r = \mathrm{d}r^2/2$ should generally be used in order to avoid confusion with the sign of r. This should be done in all expressions containing $r\mathrm{d}r$ in this work, unless noted otherwise. All integrals are solved on a cell-wise basis with a Finite Volume Method (FVM). The center cell (containing $r = 0$) is treated as a symmetric cell, with size equal to $\Delta r_c = 2r_{face}$ (this also implies $\Delta r_c^2/2 = r_{face}^2$). An important limitation arises in the spatial formulation at this point. For wall-bounded flows such as the channel and pipe flow problems discussed here, there cannot be any cell displacement at the domain boundaries. Since Eq. (8) cannot be used, Eq. (7) is inherently non-conservative in a variable density spatial formulation that involves closed lines. Nonetheless, it is always possible to force consistency of Eq. (7) if both b_k and c_k are 0. This is achieved by setting the ODT model parameter $\alpha = 0$ (see[28] for details). α is an ODT model parameter governing the redistribution (if any) of kinetic energy among the velocity components. By taking $\alpha = 0$, all of the kinetic energy remains in the streamwise velocity component and therefore, the measure preserving property of the triplet map transformation ensures conservation of streamwise momentum flux. The latter is the approach followed in this work for the S-ODT formulation.

2.2 | Deterministic momentum diffusion and enforcement of mass and energy conservation

2.2.1 | Temporal ODT Formulation

For ease of understanding, we begin the derivation of the deterministic equations with a review of the temporal formulation[22] and we discuss afterwards, based on these considerations, the suitability of a spatial formulation for closed ODT lines, i.e. lines bounded by walls, such as those present in a pipe-flow.

Formulations in this work are based on a Lagrangian framework[16]. The planar (or Cartesian) form of the equations for momentum diffusion is derived in Lignell et al[16]. Therefore, we focus on the derivation for the cylindrical form of the equations. The reader is also encouraged to consult the work of Sutherland et al.[29] for a detailed derivation of several planar ODT formulations. Before proceeding to the derivation of the deterministic equations, we stress that all of the expressions used here related to conservation of mass, momentum and energy, refer to the conservation of these quantities considering only linear effects during the deterministic advancement. During an eddy event, these quantities are satisfied by construction, as we detailed in Section 2.1.

The temporal ODT formulation (T-ODT) for pipe flow can be visualized as a fixed ODT line in the radial direction of a pipe. The temporally developing flow across the line is simulated in this formulation. Conservation of mass within a Lagrangian system Ω results in,

$$\frac{\mathrm{d}}{\mathrm{d}t} \int_{\Omega} \rho\mathrm{d}V = 0. \tag{9}$$

Here, $\mathrm{d}V$ is the volume differential in the Lagrangian system Ω, and ρ is the density. For an incompressible and radially closed system, i.e., a pipe, Eq. (9) is trivially satisfied given that neither Ω nor ρ are time-dependent functions. Likewise, any formulation and solution for energy conservation is also trivial, as it is normally the case for incompressible, adiabatic, and non-reactive

flow. We focus, therefore, in the expression for conservation of 3-D momentum, i.e. $\rho\vec{V} = \rho[u, v, w]^T$, constrained to a 1-D system[22], and following the nomenclature in Figure 1 .

$$\frac{\mathrm{d}}{\mathrm{d}t}\int_{\Omega}\rho\vec{V}\mathrm{d}\Psi = -\int_{\Psi}(\nabla\cdot p\underline{\mathbf{I}})\mathrm{d}\Psi + \int_{\Psi}(\nabla\cdot\underline{\boldsymbol{\tau}})\mathrm{d}\Psi. \tag{10}$$

In Eq. (10), p is the hydrodynamic pressure, $\underline{\boldsymbol{\tau}}$ is the shear stress tensor and $\underline{\mathbf{I}}$ is the identity matrix. We work with a cylindrical coordinate system which allows both positive and negative values of r. This is illustrated in Figure 1 . A 1-D cylindrical section, or ring, is characterized by an arbitrary swept angle $\Delta\theta$, some shell thickness Δx, and a differential radial element $\mathrm{d}r$. This leads to a volume differential element $\mathrm{d}\Psi = r\mathrm{d}r\Delta x\Delta\theta$ for any cylindrical sector resembling the one shown in Figure 1 .

We now consider streamwise momentum conservation for simplicity, i.e. the scalar version of Eq. (10) for the u component of $\vec{V}$. For the streamwise direction, the equivalent shear stress divergence in Eq. (10) takes the form $(1/r)[\partial(r\tau_{rx})/\partial r] + (1/r)(\partial\tau_{\theta x}/\partial\theta) + \partial\tau_{xx}/\partial x$. In the one-dimensional formulations used with ODT, we neglect the last two terms in the previous expression. The reader should note that $\tau_{rx} = \mu\partial u/\partial r$, whereby μ is the dynamic viscosity. For the pressure gradient, the applicable term is $\partial p/\partial x$, which can be decomposed into mean and fluctuating components, $\partial\overline{p}/\partial x$ and $\partial p'/\partial x$. The mean component is constant for incompressible channel or pipe-flow (in our case, a Fixed Pressure Gradient forcing, FPG). The effect of the fluctuating component can be ignored during the diffusion evolution, since it is part of the turbulent transport modeling. These considerations lead to,

$$\frac{\mathrm{d}}{\mathrm{d}t}\int\rho ur\mathrm{d}r = -\int\frac{\partial\overline{p}}{\partial x}r\mathrm{d}r + \int\frac{1}{r}\frac{\partial}{\partial r}\left(r\mu\frac{\partial u}{\partial r}\right)r\mathrm{d}r. \tag{11}$$

Eq. (11) is discretized by means of a Finite Volume Method (FVM). Details of the discretization and numerical method are given in APPENDIX B. We note that Eq. (11) might encounter an apparent singularity at $r = 0$. We avoid this singularity by using a symmetric center cell with fixed size, and solving a flux equalization condition for this cell (see APPENDIX B for details).

The framework developed so far also allows us to formulate an integral conservation expression for passive scalars. Here, we take the example of the passive temperature T, where all fluid properties are assumed constant, i.e. the specific heat at constant pressure c_p, the thermal conductivity λ_{th}, and the density ρ,

$$\frac{\mathrm{d}}{\mathrm{d}t}\int\rho c_p Tr\mathrm{d}r = \int\frac{1}{r}\frac{\partial}{\partial r}\left(r\lambda_{th}\frac{\partial T}{\partial r}\right)r\mathrm{d}r. \tag{12}$$

Unlike in the T-ODT momentum equation, Eq. (10), there is no pressure gradient term directly responsible for forcing the flow in Eq. (12), or at least not one which can be recognized straightforwardly. If Dirichlet boundary conditions are applied for the temperature distribution, then the initial conditions will relax into a radially uniform distribution. However, it is possible to force the flow in order to achieve a statistically steady state as in the case of the statistically steady channel flow velocity distribution. For that, a mean streamwise temperature gradient $\partial\overline{T}/\partial x$ can be calculated. An analytical derivation of $\partial\overline{T}/\partial x$ in a pipe flow is possible for the cases where the fluid properties are assumed uniform along the pipe radius[30]. This approximation is therefore valid in a pipe flow passive temperature case. For these cases, the forcing term can be added in the LHS of Eq. (12) as an advective term of the form $\int(\rho uc_p\partial\overline{T}/\partial x)r\mathrm{d}r$.

For completeness, we repeat the resulting expression for streamwise momentum conservation in the planar case (channel flow), for an ODT line coinciding with the wall-normal direction y. This expression was already derived in[16],

$$\frac{\mathrm{d}}{\mathrm{d}t}\int\rho u\mathrm{d}y = -\int\frac{\partial\overline{p}}{\partial x}\mathrm{d}y + \int\frac{\partial}{\partial y}\left(\mu\frac{\partial u}{\partial y}\right)\mathrm{d}y. \tag{13}$$

We note that for the v and w velocity components in the planar case, the resulting expressions are essentially the same as Eq. (13), except for the pressure gradient term that is ignored[16]. For the cylindrical case, however, we do not derive expressions for v and w due to theoretical considerations (see Section 3.2.1).

2.2.2 | Spatial ODT Formulation

The spatial ODT formulation (S-ODT) is a 2-D approximation of a quasi-stationary flow. In S-ODT, the ODT line moves along the streamwise direction in order to reconstruct a static 2-D picture of the flow. Considering the changes in mass only due to the net difference in mass fluxes entering and leaving the Lagrangian system Ω through the system boundary S, we can obtain the following expression for mass conservation,

$$\int_{\Omega}\nabla\cdot\left[\rho\left(\vec{V}_D - \vec{V}_S\right)\right]\mathrm{d}\Psi = 0. \tag{14}$$

$\vec{V}_S = [0, v_s, 0]^T$ is the boundary velocity of our 1-D Lagrangian system Ω, while $\vec{V}_D = [u_D, v_D, w_D]^T$ is the deformation or displacement velocity of the system, which tries to conserve mass by compensation of 3-D fluxes. For a 2-D flow, the zero thickness of our 1-D cylindrical ring allows us to accomodate incoming and outgoing momentum fluxes in the radial direction, leaving the task of balancing streamwise momentum fluxes as the solution of a streamwise parabolic-type flow. The 2-D approach supposes the homogeneity of fluid properties in spanwise or tangential direction for channel and pipe flows, respectively. With these considerations, Eq. (14) can be rewritten in a cylindrical system as,

$$\int \frac{\partial \left(\rho u_D \right)}{\partial x} r \mathrm{d}r = 0. \tag{15}$$

For open ODT domains, continuity has been traditionally solved by means of a first-order approximation in the streamwise direction (see [16,29,22] for details). For the case studied here, a first-order approximation of Eq. (15) will result, in general, in an expanded or contracted volume $\Psi_1 \neq \Psi_0$. This is physically not applicable for our wall-bounded pipe/channel systems, and therefore a new solution approach must be pursued. This problem is also present in the T-ODT formulation for cases where density is variable. The alternative approach here is motivated by the solution procedure for closed systems detailed in Medina et al [21]. For that, we resort to a differential Lagrangian formulation. The Lagrangian differential momentum Partial Differential Equation (PDE) can be written as,

$$\rho u_D \frac{\mathrm{d}u}{\mathrm{d}x} = -\frac{\partial \overline{p}}{\partial x} + \frac{1}{r} \frac{\partial}{\partial r} \left(r \mu \frac{\partial u}{\partial r} \right). \tag{16}$$

Due to the spatial formulation, we defined the Lagrangian derivative operator $\mathrm{d}/\mathrm{d}t$ as $(u_D)\mathrm{d}/\mathrm{d}x$. Therefore, there exists an implicit change of variables $u_D = \mathrm{d}x/\mathrm{d}t$. Now consider again the cylindrical coordinate system from Figure 1 . Due to the 2-D formulation, we can choose the shear stress divergence as $(1/r)[\partial(r\tau_{rx})/\partial r] + \partial\tau_{xx}/\partial x$ for the u velocity component. Although this is theoretically consistent, preserving both the radial and axial terms in the shear stress results in an elliptic PDE. This is not solvable as a spatial marching problem, and it is also not clear how this would affect the instantaneous eddy event implementation. This is one of the main limitations of the S-ODT formulation [28]. For this reason, the axial shear stress gradient is also neglected in our spatial formulation. A similar reasoning forbids the use of a variable axial pressure gradient $\partial p/\partial x$. At most, a constant forcing FPG $\partial \overline{p}/\partial x$ can be imposed, as in the T-ODT formulation.

Simultaneous enforcement of mass and energy conservation is given by the zero divergence condition in the zero Mach number limit. However, this is again another limitation in our spatial formulation for a pipe flow, since the divergence condition for a 2-D flow mandates $\partial u_D/\partial x + (1/r)[\partial(r v_D)/\partial r] = 0$. Note that we use the velocity $\vec{V}_D$ in the divergence condition, motivated by the understanding of $\vec{V}_D$ as a flux velocity, $\vec{V}_D \neq \vec{V}$, where $\vec{V}$ is the Lagrangian velocity of the system. In order to find an expression for $\partial u_D/\partial x$ that can be substituted in the divergence condition, an elliptic operator such as the pressure in the streamwise momentum equation must be applied. Since we required a constant axial pressure gradient, as in the temporal formulation, we can expect that $\partial u_D/\partial x$ in the divergence condition will only be satisfied in the forced fully developed regime, when $u_D = u$. Therefore, we can not consider the 2-D divergence condition due to its relation with the elliptic character of the flow. Instead, a 1-D divergence condition $(1/r)[\partial(r v_D)/\partial r] = 0$, must be enforced. However, this is again trivially satisfied for a constant radial velocity v_D, implying a cancellation of the radial momentum or radial mass flux, thus automatically preserving the radius constraint of the pipe.

Since no divergence condition for u_D can be used, we must change the weak differential formulation into a strong formulation for $\mathrm{d}(\rho u_D u)/\mathrm{d}x$. Here, however, we take then $u_D = u$, as commented before. Since the density is constant, we rewrite the differential streamwise momentum flux equation as,

$$\rho \frac{\mathrm{d}u^2}{\mathrm{d}x} = -\frac{\partial \overline{p}}{\partial x} + \frac{1}{r} \frac{\partial}{\partial r} \left(r \mu \frac{\partial u}{\partial r} \right). \tag{17}$$

The numerical method used to solve Eq. (17) is detailed in APPENDIX B. We note that a solution for Eq. (17) might involve positive and negative roots for the streamwise velocity u. However, other velocity components should evolve independently during diffusion. Also, due to the application of the FPG, strictly positive velocity profiles will remain positive, thus allowing the consistency with the spatial marching solution approach.

For completeness, the momentum conservation for the spatial formulation in the planar case (channel flow) is

$$\rho \frac{\mathrm{d}u^2}{\mathrm{d}x} = -\frac{\partial \overline{p}}{\partial x} + \frac{\partial}{\partial y} \left(\mu \frac{\partial u}{\partial y} \right). \tag{18}$$

We do not consider the resulting terms for the v and w momentum equations, since our spatial eddy event formulation forbids the use of more than one velocity component for the channel and pipe-flow cases (see Section 2.1). The temperature scalar

equation is not considered in the spatial formulation since we only work with Dirichlet temperature boundary conditions. In order to force a statistically steady temperature distribution in the spatial formulation, a heat flux boundary condition is required at the wall. This is because imposing a fixed $\partial \overline{T}/\partial x$ as a source term is in conflict with solving an equation for streamwise temperature advancement in the spatial formulation. Rather, the heatflux, from which the term $\partial \overline{T}/\partial x$ is calculated, must be used as a boundary condition.

3 | STATISTICAL QUANTITIES IN ODT REALIZATIONS

As shown in Kerstein et al.[17], equivalences between statistical DNS and ODT quantities can be made based on the comparison of the mean ODT and Reynolds-Averaged Navier-Stokes (RANS) momentum equations. In this section we illustrate these equivalences from the point of view of Reynolds stresses and Turbulent Kinetic Energy (TKE) budgets for the planar case, summarizing the findings in Kerstein et al[17]. Afterwards, we introduce the equivalences for the cylindrical case. For convenience, an index notation is used for velocity components in this section. All of the findings in this section can be generalized for the passive scalar conservation laws.

3.1 | Planar Reynolds Stresses and TKE budgets

3.1.1 | Planar T-ODT formulation

A mathematical representation of the generalized T-ODT momentum evolution equation in the planar case is given by the differential expression of Eq. (13) in an Eulerian framework, with constant density ρ and assumed kinematic viscosity ν,

$$\frac{\partial u_1}{\partial t} = -\frac{1}{\rho}\frac{\partial \overline{p}}{\partial x} + \nu \frac{\partial^2 u_1}{\partial y^2} + M_1 + K_1. \tag{19}$$

We use $u_1 = u$ in the index notation. Here, the advective term has been omitted due to the effective zero mean advection of the flow and the turbulent advection representation by eddy events. $M_1 + K_1$ stands for the combined effect of the triplet-map (M_1), pressure scrambling (S_1) and turbulent transport contribution (T_1) in the ODT velocity component u_1 [17]. According to the definition of the model, K_1 is selected in such a way that $K_1 = T_1 + S_1$, where $S_1 = 0$ is defined for convenience due to the absence of pressure scrambling contributions in the mean Navier-Stokes momentum equation[17]. It is possible to compare Eq. (19) with the steady state channel flow RANS momentum equation,

$$0 = -\frac{1}{\rho}\frac{\partial \overline{p}}{\partial x} + \nu \frac{\partial^2 \overline{u_1}}{\partial y^2} - \frac{\partial \overline{u_1' u_2'}}{\partial y}. \tag{20}$$

In this context, the mean T-ODT momentum evolution is,

$$\frac{\partial \overline{u_1}}{\partial t} = -\frac{1}{\rho}\frac{\partial \overline{p}}{\partial x} + \nu \frac{\partial^2 \overline{u_1}}{\partial y^2} + \overline{M_1} + \overline{T_1}. \tag{21}$$

Here, we have used the standard temporal Reynolds average operator, noted in general with overbars, to achieve the statistically stationary state on the LHS. It is then straightforward to verify that the equivalence of the Reynolds stress component $\overline{u_1' u_2'}$ in the T-ODT planar case is given by,

$$-\overline{u_1' u_2'} = \int_y^{y_w} (\overline{M_1} + \overline{T_1}) \mathrm{d}y^*. \tag{22}$$

Here, the y_w integration boundary refers to the position of the wall. Operationally, $\overline{M_1} + \overline{T_1}$ is defined by changes in the velocity profiles due to eddies. Considering the stochastic interaction in Eq. (19) within a given interval of time Δt in which eddies are deemed to occur,

$$\frac{\sum (\Delta u_1)_{eddies}}{\Delta t} = M_1 + T_1. \tag{23}$$

Averages $\overline{M_1} + \overline{T_1}$ can then be constructed based on the cumulative sum of changes in the u_1 velocity profiles due to eddies.

For the evaluation of the TKE Budgets, the starting point is the momentum evolution equation, Eq. (19), multiplied by the u_1 velocity component (kinetic energy of the u_1 velocity component),

$$\frac{1}{2}\frac{\partial u_1^2}{\partial t} = -\frac{u_1}{\rho}\frac{\partial \overline{p}}{\partial x} + \nu u_1 \frac{\partial^2 u_1}{\partial y^2} + M_{11} + K_{11} \rightarrow \frac{\partial u_1^2}{\partial t} = -\frac{2u_1}{\rho}\frac{\partial \overline{p}}{\partial x} + \nu \frac{\partial^2 u_1^2}{\partial y^2} - 2\nu \left(\frac{\partial u_1}{\partial y}\right)^2 + M_{11} + K_{11}. \tag{24}$$

Here, $M_{11} + K_{11}$ is the sum of the mapping M_{11}, transport T_{11} and pressure scrambling S_{11} contributions to the kinetic energy of the u_1 velocity component.

Averaging Eq. (24) and using the identities $\overline{u_1^2} - \overline{u_1}^2 = \overline{u_1'^2}$, $I_1 = \int (\overline{M_1 + T_1}) dy$, and $I_{11} = \int (\overline{M_{11} + T_{11}}) dy$, along with Eq. (21) multiplied by $2\overline{u}_1$, an equation for the average of the square of the fluctuation velocity u_1' can be obtained[17],

$$\frac{\partial \overline{u_1'^2}}{\partial t} = \nu \frac{\partial^2 \overline{u_1'^2}}{\partial y^2} - 2\nu \overline{\left(\frac{\partial u_1'}{\partial y}\right)^2} + \left[\frac{\partial}{\partial y}\left(I_{11} - 2\overline{u}_1 I_1\right) + \overline{S_{11}}\right] + 2I_1 \frac{\partial \overline{u}_1}{\partial y}. \tag{25}$$

Comparing Eq. (25) to the generalized TKE equation in a Cartesian coordinate system (see, e.g., Eq. (5.164) from Pope, 2011[10]), it is possible to deduce that an accurate representation of the flow can be obtained by summing up the contributions by $\overline{u_1'^2}, \overline{u_2'^2}, \overline{u_3'^2}$, such that TKE $= (1/2)(\overline{u_1'^2} + \overline{u_2'^2} + \overline{u_3'^2})$. That is, $\alpha \neq 0$ in the ODT model. The most reasonable choice is to consider $\alpha = 2/3$, which implies equal available energy redistribution after an eddy event. The equations for $\overline{u_2'^2}, \overline{u_3'^2}$ are similar to Eq. (25), with $\overline{u_2'^2}, \overline{u_3'^2}$ substituting $\overline{u_1'^2}$. As in Kerstein et al.[17], the resulting TKE budgets for production P and dissipation D are,

$$P = \sum_k I_k \frac{\partial \overline{u_k}}{\partial y}, \quad D = \sum_k \nu \overline{\left(\frac{\partial u_k'}{\partial y}\right)^2}. \tag{26}$$

3.1.2 | Planar S-ODT formulation

The instantaneous momentum evolution in the spatial formulation is, following from Eq. (18),

$$\frac{\partial u_1^2}{\partial x} = -\frac{1}{\rho}\frac{\partial \overline{p}}{\partial x} + \nu \frac{\partial^2 u_1}{\partial y^2} + M_1 + T_1. \tag{27}$$

Averaging Eq. (27), by means of a streamwise Reynolds average operator, analogous to the temporal average operator, results in

$$\frac{\partial \overline{u_1^2}}{\partial x} = -\frac{1}{\rho}\frac{\partial \overline{p}}{\partial x} + \nu \frac{\partial^2 \overline{u}_1}{\partial y^2} + \overline{M_1} + \overline{T_1}. \tag{28}$$

We note that for a fully developed incompressible channel (or pipe) flow, the equivalence between temporal and spatial homogeneity allows us the application of the previously mentioned streamwise Reynolds average operator. Comparing this expression with the traditional Navier-Stokes equation for momentum conservation in an Eulerian framework, results in the equivalence $\overline{M_1} + \overline{T_1} = \partial \overline{u_1 u_2}/\partial y$. We can then deduce, equivalent to T-ODT,

$$\overline{u_1' u_2'} = \overline{u_1 u_2} - \overline{u_1}\,\overline{u_2} = \int_{y_w}^y \overline{M_1 + T_1} dy^*. \tag{29}$$

Note that in Eq. (29), the term $\overline{u_1}\,\overline{u_2}$ was neglected due to the absence of mean advection in the cross-wise direction. In this case, the Reynolds stress component $\overline{u_1' u_2'}$ is also given by Eq. (22). $\overline{M_1} + \overline{T_1}$ is calculated accounting for the changes in the u_1^2 velocity profiles, in contrast to Eq. (23) in the temporal case.

$$\frac{\sum \left(\Delta u_1^2\right)_{eddies}}{\Delta x} = M_1 + T_1. \tag{30}$$

The TKE flux equation based on the u_1 velocity component is in this case very similar to the T-ODT formulation. For the spatial formulation, we focus here only on the production and dissipation budgets. Following a similar derivation procedure and accounting for $\alpha = 0$ in the spatial formulation, it is then possible to obtain the corresponding expressions for the production P and dissipation D,

$$P = I_1 \frac{\partial \overline{u}_1}{\partial y}, \quad D = \nu \overline{\left(\frac{\partial u_1'}{\partial y}\right)^2}. \tag{31}$$

3.2 | Cylindrical Reynolds Stresses and TKE budgets

3.2.1 | Cylindrical T-ODT formulation

We now introduce for the first time the derivation of the ODT TKE equation for the cylindrical formulation. This derivation allows a very important insight regarding assumptions done in the cylindrical ODT formulation. In order to derive the cylindrical TKE budgets, we follow the same methodology as in the planar case.

The generalized T-ODT cylindrical momentum equation is given in this case by the differential version of Eq. (11) in an Eulerian framework,

$$\frac{\partial u_1}{\partial t} = -\frac{1}{\rho}\frac{\partial \overline{p}}{\partial x} + \frac{\nu}{r}\frac{\partial}{\partial r}\left(r\frac{\partial u_1}{\partial r}\right) + M_1 + T_1. \tag{32}$$

Eq. (32) is compared with the steady pipe flow RANS momentum evolution,

$$0 = -\frac{1}{\rho}\frac{\partial \overline{p}}{\partial x} + \frac{\nu}{r}\frac{\partial}{\partial r}\left(r\frac{\partial \overline{u_1}}{\partial r}\right) - \frac{\partial \overline{u_1' u_2'}}{\partial r} - \frac{\overline{u_1' u_2'}}{r}. \tag{33}$$

Here $\overline{u_1' u_2'} = \overline{u'v'}$. Therefore, the mean T-ODT momentum evolution is in this case,

$$\frac{\partial \overline{u_1}}{\partial t} = -\frac{1}{\rho}\frac{\partial \overline{p}}{\partial x} + \frac{\nu}{r}\frac{\partial}{\partial r}\left(r\frac{\partial \overline{u_1}}{\partial r}\right) + \overline{M_1} + \overline{T_1}. \tag{34}$$

Comparing Eqs. (33) and (34), the Reynolds stress component $\overline{u_1' u_2'}$ in the T-ODT cylindrical case is then formally defined by

$$-\overline{u_1' u_2'} = \frac{1}{r}\int_r^R (\overline{M_1} + \overline{T_1}) r^* \mathrm{d}r^* = I_1. \tag{35}$$

$\overline{M_1} + \overline{T_1}$ can be calculated just like in the planar case by means of Eq. (23).

The kinetic energy evolution equation for the u_1 axial velocity component is,

$$\frac{1}{2}\frac{\partial u_1^2}{\partial t} = -\frac{u_1}{\rho}\frac{\partial \overline{p}}{\partial x} + \nu\frac{u_1}{r}\frac{\partial}{\partial r}\left(r\frac{\partial u_1}{\partial r}\right) + M_{11} + K_{11},$$
$$\frac{\partial u_1^2}{\partial t} = -\frac{2u_1}{\rho}\frac{\partial \overline{p}}{\partial x} + \frac{\nu}{r}\frac{\partial u_1^2}{\partial r} + \nu\frac{\partial^2 u_1^2}{\partial r^2} - 2\nu\left(\frac{\partial u_1}{\partial r}\right)^2 + M_{11} + K_{11}. \tag{36}$$

Analogous to the planar case, the TKE equation based on the u_1 axial velocity component can be obtained as

$$\frac{\partial \overline{u_1'^2}}{\partial t} = \frac{\nu}{r}\frac{\partial}{\partial r}\left(r\frac{\partial \overline{u_1'^2}}{\partial r}\right) - 2\nu\overline{\left(\frac{\partial u_1'}{\partial r}\right)^2} + \frac{1}{r}\frac{\partial}{\partial r}\left[r\left(I_{11} - 2\overline{u_1}I_1\right)\right] + 2I_1\frac{\partial \overline{u_1}}{\partial r} + \overline{S_{11}}. \tag{37}$$

Here, we have used the identity $I_{11} = (1/r)\int(\overline{M_{11}} + \overline{T_{11}})r\mathrm{d}r$. A subtraction and addition of $2I_1\partial\overline{u_1}/\partial r$ is required, just as in the planar case, in order to obtain the final expression. It is interesting to note that in comparing this expression to the generalized TKE equation in cylindrical coordinates (see, e.g. Eqs. (B.31-B.33) in Shiri, 2010[31]), a series of terms could be missing in the model if we try to generalize Eq. (37) to the radial and tangential fluctuating velocity components $\overline{u_2'^2}$ and $\overline{u_3'^2}$. In a cylindrical coordinate system, the diffusion evolution equations for u_2 and u_3 do not have in general the same terms as u_1 (in contrast to the planar case). In this sense, the budget terms obtained by analyzing Eq. (37) represent only radial fluxes, a radial TKE production term, and interestingly enough, a planar dissipation component. In order to be able to obtain a more consistent representation of the TKE budget terms in a vector formulation, different equations for the radial and tangential velocity components would be required, not only in the diffusion evolution PDEs, but possibly in the same eddy implementation procedure. Although this is a minor technicality, given that the non-streamwise velocity components are just interpreted as energy containers in the ODT vector formulation[17], we maintain a consistent representation by applying a scalar treatment of the momentum and energy, i.e., we restrain our choice of α in the T-ODT cylindrical formulation to 0. Nonetheless, this is an aspect that could be studied in future work.

Due to the before mentioned shortcomings, and in order to guarantee consistency, we conclude in this section that for the case of the cylindrical model formulation, at least in this study, the ODT model parameter α should be set to 0. With this consideration, the radial and tangential velocity components remain 0 and the TKE budgets are consistently represented by Eq. (37) only.

The production and dissipation terms are consequently defined based on Eq. (37),

$$P = I_1\frac{\partial \overline{u_1}}{\partial r}, \quad D = \nu\overline{\left(\frac{\partial u_1'}{\partial r}\right)^2}. \tag{38}$$

3.2.2 | Cylindrical S-ODT formulation

Similar to the temporal formulation, the generalized spatial ODT cylindrical momentum evolution for u_1 is given by

$$\frac{\partial u_1^2}{\partial x} = -\frac{1}{\rho}\frac{\partial \overline{p}}{\partial x} + \frac{\nu}{r}\frac{\partial}{\partial r}\left(r\frac{\partial u_1}{\partial r}\right) + M_1 + T_1. \tag{39}$$

Averaging Eq. (39), results in

$$\frac{\overline{\partial u_1^2}}{\partial x} = -\frac{1}{\rho}\frac{\partial \overline{p}}{\partial x} + \frac{\nu}{r}\frac{\partial}{\partial r}\left(r\frac{\partial \overline{u_1}}{\partial r}\right) + \overline{M_1} + \overline{T_1}. \tag{40}$$

As in the planar case, $\overline{u_1' u_2'} = \overline{u_1 u_2} - \overline{u_1}\,\overline{u_2}$, where $\overline{u_2} = 0$ due to the absence of mean advection in the radial direction. Consequently, the Reynolds stress component $\overline{u_1' u_2'}$ is calculated as in the temporal formulation by Eq. (35). The calculation of $\overline{M_1} + \overline{T_1}$ is done exactly as in the planar spatial case via Eq. (30). The production P and dissipation D budgets for $\alpha = 0$ (one velocity component) are given by Eq. (38).

4 | INCOMPRESSIBLE PIPE AND CHANNEL FLOW RESULTS FOR MODERATE TO LARGE REYNOLDS NUMBERS

4.1 | Flow configuration

The details of the simulations performed are given in Tables 1 and 2 . All simulations are initialized with constant velocity profiles. Simulations are run without statistical data gathering until the transient effects disappear. Afterwards, online averages and cumulative sums are gathered and updated after eddy events and after diffusion catch-up events, as discussed in Section 3. The data is gathered until the statistical convergence of the desired quantities is achieved.

The ODT code used in this work is written in C++ and utilizes an adaptive grid[22]. The most important parameters controlling the mesh adaption process are the minimum and maximum cell size allowed during the adaption dxmin and dxmax, as well as the grid density factor controlling the approximate number of cells generated after the adaption process gDens. The factor gDens determines the number of cells to be generated based on the redistribution calculated by the equipartition of arc lengths in a given adaption interval[16]. These parameters are also given in Tables 1 and 2 . Another parameter related to the effects of mesh adaption in the cylindrical formulation, DATimeFac, is explained and evaluated in Section 4.2.

TABLE 1 Parameters used for channel flow simulations (Temporal and Spatial formulation). η refers to the Kolmogorov length scale.

Parameter (Case)	$\mathrm{Re}_\tau = 590$ (A)	$\mathrm{Re}_\tau = 934$ (B)	$\mathrm{Re}_\tau = 2003$ (C)
Domain Length L (m)	2.0	2.0	2.0
Density ρ (kg/m³)	1.0	1.0	1.0
Kinematic viscosity ν (m²/s)	1.6949×10^{-3}	1.0707×10^{-3}	0.9985×10^{-3}
FPG Forcing $\partial \overline{p}/\partial x$ (Pa/m)	-1.0	-1.0	-4.0
Mesh adaption parameter dxmin = $\eta/3$ (m)	5.6496×10^{-4}	3.5688×10^{-4}	1.6642×10^{-4}
Mesh adaption parameter dxmax (m)	0.04	0.04	0.04
Mesh adaption parameter gDens	80.0	80.0	80.0
Mesh adaption parameter DATimeFac	4.0	4.0	4.0
ODT parameter C	6.5 (T-ODT) / 3.0 (S-ODT)		
ODT parameter Z	300.0 (T-ODT) / 100.0 (S-ODT)		
ODT parameter α	$2/3 \approx 0.6667$ (T-ODT) / 0.0 (S-ODT)		
Eddy-size PDF L_{max} (normalized by L)	$1/3 \approx 0.3333$		

TABLE 2 Parameters used for pipe flow simulations (Temporal and Spatial formulation). η refers to the Kolmogorov length scale and Δr_C to the assumed symmetric center cell size.

Parameter (Case)	$Re_\tau = 590$ (A)	$Re_\tau = 934$ (B)	$Re_\tau = 2003$ (C)
Domain Length $2R$ (m)	2.0	2.0	2.0
Density ρ (kg/m^3)	1.0	1.0	1.0
Kinematic viscosity ν (m^2/s)	1.8182×10^{-3}	1.0×10^{-3}	0.9985×10^{-3}
FPG Forcing $\partial \overline{p}/\partial x$ (Pa/m)	-2.0	-2.0	-8.0
Mesh parameter Δr_C (m)	0.04	0.0222	0.0111
Mesh adaption parameter dxmin $= \eta/3$ (m)	6.0606×10^{-4}	3.3333×10^{-4}	1.6642×10^{-4}
Mesh adaption parameter dxmax (m)	0.04	0.04	0.04
Mesh adaption parameter gDens	80.0	80.0	80.0
Mesh adaption parameter DATimeFac	4.0	7.3	14.5
ODT parameter C	5.0 (T-ODT) / 3.0 (S-ODT)		
ODT parameter Z	350.0 (T-ODT) / 100.0 (S-ODT)		
ODT parameter α	0.0		
Eddy-size PDF L_{max} (normalized by L)	$1/3 \approx 0.3333$		

Optimal ODT C and Z parameters are shown in Tables 1 and 2, along with the suggested value of L_{max} for the assumed eddy size PDF used by ODT, as explained in Section 2.1. The C and Z parameters were obtained after a model calibration study detailed in APPENDIX C. Influence due to the assumed value of L_{max} is investigated in Section 4.2.

Despite the parameters mentioned above and listed in Tables 1 and 2, we emphasize that, as discussed in Section 2.1, the only effective ODT model parameters are C and Z. As it has been proved in previous ODT investigations [15,32], there exists a Reynolds number dependence of the Z parameter for the bulk region of the velocity profile. Additionally, for lower Reynolds numbers, there exists a dependence on the ODT parameter C, given that a C value of 0 is indicative of a laminar flow (no eddy events implemented). For this work, however, we found an excellent Reynolds number scaling for the calibrated (and therefore Re_τ independent) C and Z values between $Re_\tau \approx 550$ and $Re_\tau \approx 2000$, as shown in APPENDIX C. This can be related to the continued collapse of the scaled profiles at larger Reynolds numbers. Lignell et al. [22] also show results comparing ODT round jets and pipe flow results as evidence of this collapse and of the insensitivity of the mean velocity profiles to ODT parameters at large bulk Reynolds numbers ($Re_b \approx 100,000$). Mesh adaption related parameters are only sensitive to the results for grid dependent studies, as in any non-resolved, implicit LES. However, as we will show in Section 4.2, some of these mesh adaption related parameters may have an exaggerated effect on the numerical diffusion, if an improper scaling is considered.

4.2 | Sensitivity to L_{max} and DATimeFac parameters

4.2.1 | Influence of the parameter L_{max}

As we will show, the qualitative influence of L_{max} on the mean velocity profiles is generally the same for all Reynolds numbers evaluated. As shown in Schmidt et al. [19], L_{max} affects the mean velocity profiles for the channel flow case in the outermost region from the wall. This parameter was estimated to have an optimal normalized value of 0.5 [19]. Krishnamoorthy [18] also verified the influence of L_{max} on the pipe flow configuration, estimating an optimal normalized value of 0.3333.

Figure 2 shows the influence of L_{max} on the T-ODT formulation for channel and pipe flow. In this study we chose the same value of L_{max} for both the pipe and channel flow configurations, motivated exclusively by consistency between both formulations. We note that it is possible to obtain calibrated parameters that match DNS data with the normalized value of $L_{max} = 0.5$ [19,15], however, we did not do this due to consistency with the cylindrical formulation. It is possible to obtain calibrated parameters that reasonably match DNS data with a normalized value of L_{max} equal to 0.3333 for both the planar and cylindrical configurations. Qualitatively, L_{max} has the same impact in both the channel and pipe flow configurations. Generally speaking, larger values of L_{max} seem to promote more mixing close to the centerline, thus resulting in a flatter velocity profile near the centerline.
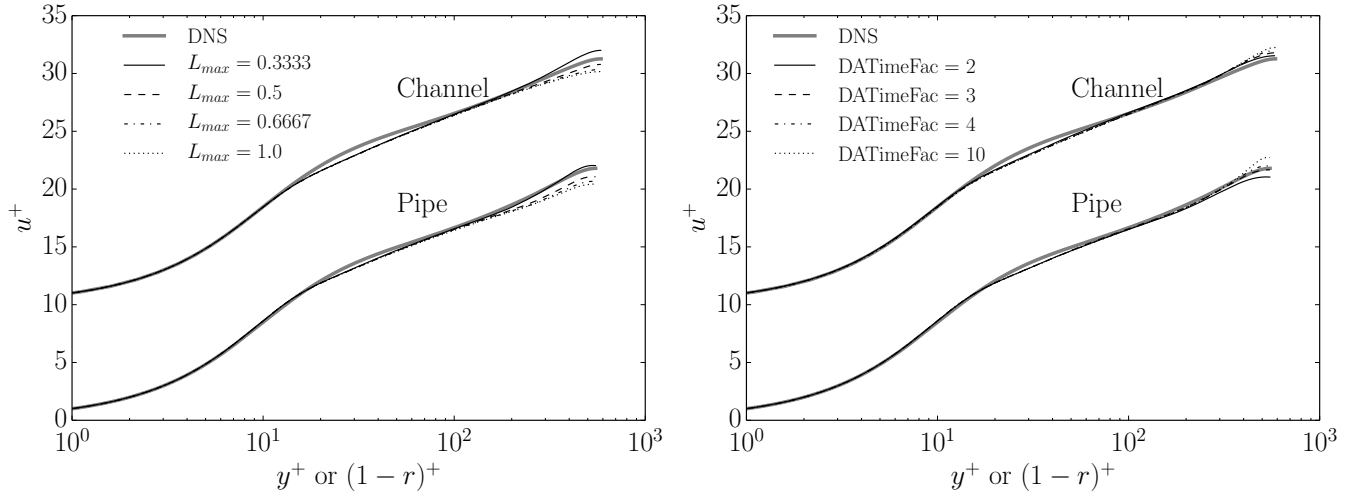
FIGURE 2 Influence of the ODT parameters L_{max} and DATimeFac on the normalized wall-normal pipe and channel flow mean velocity profiles. Pipe flow results are shown for $Re_\tau = 550$ and compared to DNS results from Khoury et al[24]. Channel flow results are shown for $Re_\tau = 590$ and compared to DNS results from Moser et al[25]. Channel flow results have been shifted upwards for better visualization: a) shows the influence of L_{max} and b) the influence of DATimeFac.

4.2.2 | Influence of the parameter DATimeFac

Despite being seldomly discussed in ODT simulations, one last parameter of interest has been calibrated in this work. This parameter is linked to the performance of the mesh adaption process. Although it was not mentioned in Section 2.1, we remark that the diffusion catch-up step, which is characteristic of ODT, occurs every time an eddy is implemented, but also anytime that the diffusion CFL time-step Δt_{CFL} is exceeded without any eddy being selected. The diffusion CFL time-step in the deterministic advancement of an ODT channel flow is given by,

$$\Delta t_{CFL} = \frac{\text{dxmin}^2}{\nu} = \frac{\eta^2}{9\nu}, \tag{41}$$

where dxmin is the minimum cell size allowed by the mesh adaption process and η is the Kolmogorov length scale (we assume a resolution dxmin $= \eta/3$).

The DATimeFac parameter works as a switch to allow mesh adaption after sufficient time has elapsed without any single eddy being implemented, i.e. time elapsed just performing diffusion steps. For low Reynolds numbers, such as the $Re_\tau = 550$ case evaluated in this work, successive diffusion steps are prone to occur. Also, due to the flow configuration, the probability of eddies being selected in the region close to the centerline is lower. Both of these factors contribute to a larger impact of the mesh adaption process in the region close to the centerline.

Operationally, we can define the DATimeFac as a ratio between a characteristic eddy implementation time-scale and the diffusion CFL time-step. The mesh adaption procedure should be called if we exceed a threshold $\Delta t_d > (\text{DATimeFac})\left(\Delta t_{CFL}\right)$, where Δt_d is a time interval proportional to some characteristic eddy implementation time-scale. For channel and pipe flows, this characteristic eddy implementation time-scale is proportional to δ/u_τ, the ratio between the half-height of the channel, or pipe Radius, and the friction velocity.

$$\text{DATimeFac} \sim \frac{\Delta t_d}{\Delta t_{CFL}} \rightarrow \text{DATimeFac} = \frac{\beta \delta}{u_\tau} \frac{9\nu}{\eta^2}. \tag{42}$$

In Eq. (42) we have substituted Eq. (41) and inserted a proportionality constant β for Δt_d. Eq. (42) allows us to find a scaling law for DATimeFac as a function of the friction Reynolds number in channel and pipe flows, given that $u_\tau = Re_\tau \nu/\delta$. For two different friction Reynolds numbers in similar geometric channel or pipe configurations, the relation between two different DATimeFac factors is,

$$\text{DATimeFac}_2 = \text{DATimeFac}_1 \frac{Re_{\tau,2}}{Re_{\tau,1}}. \tag{43}$$
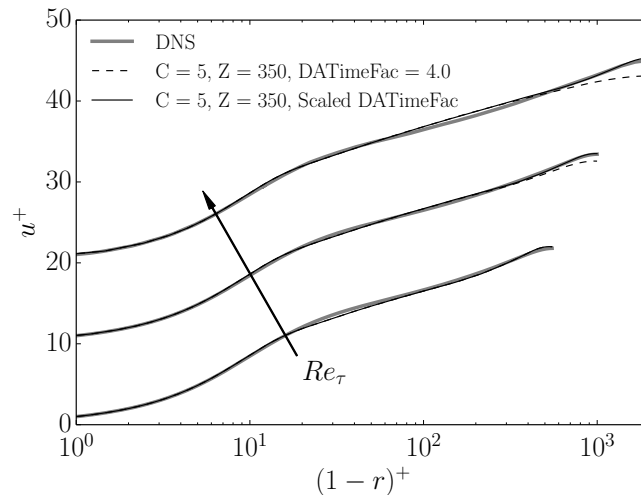
FIGURE 3 Influence of DATimeFac scaling on the normalized wall-normal pipe flow mean velocity profile for $Re_\tau = 550, 1000, 2003$. DNS results from Khoury et al. [24] ($Re_\tau = 550, 1000$) and Chin et al. [23] ($Re_\tau = 2003$) are shown for reference. The results for increasing Reynolds numbers have been shifted upwards in the plot for better visualization.

Figure 2 shows the influence of DATimeFac in the channel and pipe flow simulations. As in the case of the parameter L_{max}, the influence of DATimeFac is approximately the same for both the channel and pipe-flow configurations. Based on this analysis, we select the value of DATimeFac = 4 as the optimal one for all simulations. We note that the influence of DATimeFac is almost negligible in the planar formulation.

We can now calibrate the factor DATimeFac for a given $Re_{\tau,1}$ and then find the equivalent DATimeFac$_2$ corresponding to another $Re_{\tau,2}$, as per Eq. (43). This is the approach followed in this work, where the DATimeFac calibration was performed for Case A in the channel and pipe flow, obtaining the appropriate value of DATimeFac = 4. Evaluating the pipe flow and channel flow configurations, it was found, however, that the planar (channel) configuration was completely insensitive to the DATimeFac scaling with the friction Reynolds number scaling. This is not a surprise, since no planar ODT investigation so far has discussed this parameter. Influence of the scaling was found to be significant in the cylindrical configuration, as shown in Figure 3 .

We attribute the DATimeFac scaling sensitivity in ODT pipe flow to the center cell treatment, as described in APPENDIX B and APPENDIX D. The forcing of the fixed center cell size provokes an anomaly caused by the mesh adaption after eddy implementation. This does not occur in the planar formulation. Due to this reason, a delicate balance between the center cell size and the adaption frequency must be considered in order to achieve a consistent scaling, as in the planar formulation. Finally, we note that, although the derivation for the DATimeFac sensitivity was done on the grounds of the temporal formulation, we have verified in our simulations that it also influences the spatial simulations in the same way. We have verified, in fact, that it is also possible to apply the same scaling law from Eq. (43) in our spatial formulation.

4.3 | Comparison between channel and pipe flow statistics

Statistics gathered from the T-ODT temporal and S-ODT spatial formulation comparing pipe and channel flow simulations are shown in this section. All of the results shown here were obtained with the optimal calibrated parameters presented in Tables 1 and 2 .

The ODT spatial formulation developed in this work is used to show that both T-ODT and S-ODT formulations are consistent and capable of delivering approximately the same results, something that has never been investigated before. This is a direct analogy of evaluating snapshots in time (for spatially invariant flows) or in space (for temporal invariant flows) with the purpose of constructing average behaviors. For a fully developed flow, such as the pipe and channel flows evaluated in this work, both methods should yield approximately the same statistical results.

The reader should note, however, that simulation times and ODT parameters such as C or Z might vary between the spatial and temporal formulation. This is based on the subtle differences regarding the eddy implementation procedure and the different PDEs that are being solved during the deterministic momentum diffusion evolution. It is also important to stress the fundamental

restriction for spatial formulations in ODT, namely, the exclusive treatment of parabolic problems. This leads to simplifications and assumptions made during the derivation of the equations, which are not necessarily the same ones as in the temporal formulation.

Traditional spatial formulations in ODT aim to replicate spatially evolving flows, which would translate, in the context of the pipe and channel flow cases evaluated here, in boundary layer type-flows with a spatially varying friction Reynolds number. This is not the case of the spatial formulation introduced in this work, since we are using a FPG forcing. For this reason, our spatial simulations resemble the temporal simulations: an ensemble average over realizations at a same spatial coordinate is exactly equivalent to an ensemble average over accumulated realizations in space. The latter is the averaging philosophy applied in this work for the spatial simulations. In the temporal simulations, an ensemble average over accumulated realizations in time is considered.

4.3.1 | Mean velocity profiles and RMS velocity profiles

The results for the normalized wall-normal mean velocity profile are summarized in Figure 4 for the different Reynolds numbers evaluated in this work. Note that, as in the DNS from Chin et al.[23] and due to the available DNS results in the literature, the friction Reynolds numbers from $Re_\tau = 590$ and $Re_\tau = 934$ for the channel flow simulations are compared to the $Re_\tau = 550$ and $Re_\tau = 1000$ pipe flow simulations. Although these Reynolds numbers from the channel and pipe flow configurations are not exactly the same, the differences in the comparison are expected to be negligible.

As shown previously for channel flow simulations[15,19], ODT reasonably reproduces the mean velocity profile behavior. The comparison between DNS and ODT data for pipe flow and channel flow shows that ODT simulations are able to match the DNS behavior very well in the viscous layer, the inner buffer layer and the logarithmic layer. Differences can be noted between ODT and DNS in the meso layer and outer buffer layer. These differences are expected, since the buffer layer is mainly influenced by large scale structures not represented in ODT[15]. The buffer layer representation, however, is improved in ODT with increasing values of Re_τ, as seen by comparing the different profiles in Figure 4 . This is due to the achievement of an asymptotically turbulent regime. In such regimes, ODT is expected to behave better given that large scale motions become less and less relevant[19].

By comparing ODT results between pipe and channel flow simulations, it is immediately noticeable that the similarity of the flows is maintained, just as in the DNS. Considering that the recent cylindrical formulation in ODT has not undergone extensive validation studies, this is an aspect worth stressing. Also, the similarity of the channel and pipe flows is somehow reflected on the chosen optimal C and Z values for the planar and cylindrical configurations, given that these values are close to each other. As seen in the DNS results, the ODT behavior for channel flow shows an earlier departure into the logarithmic layer in comparison to pipe flow.

With the parameters selected for the spatial formulation, the obtained mean velocity profiles lie generally below those of the temporal formulation. A larger gradient of the velocity profile is noticeable in the logarithmic layer, close to the channel and pipe centerlines. Note that these results were obtained just by tuning the C and Z parameters in order to achieve a reasonable match to the DNS data, while preserving model parameters which were very close to their counterparts of the temporal formulation. The same L_{max} and DATimeFac parameters from the temporal formulation were used for the spatial formulation.

It is also interesting to note that, at least for case A, the optimal values for the parameters C and Z are the same ones for both the pipe and channel flow configurations in the spatial formulation ($C = 3.0$ and $Z = 100.0$).

A comparison of the RMS velocity profiles for ODT and DNS channel and pipe flow simulations is shown next in Figure 5 . In contrast to the mean velocity profiles, the ODT behavior is significantly different from the DNS data, consistent with previous ODT investigations[15,16]. In the viscous layer, ODT results are slightly shifted in a parallel manner compared to DNS results. Discrepancies between ODT and DNS become more pronounced after the RMS peak close to the wall is achieved. ODT results for channel and pipe flow show similar behavior. The RMS double peak in T-ODT results is an intrinsic feature of the triplet maps used in the model[16], and it must not be confused with the common second peak discussion for pipe flow simulations in large Reynolds numbers regimes[1,23]. We note that the double peak obtained in the S-ODT formulation is significantly reduced and almost disappears from the profile. This could be seen as an advantage against the temporal formulation. However, the position of the peak in the spatial formulation is shifted in comparison to the DNS results.

Since the ODT parameter α was set to 0 in the pipe flow T-ODT simulations (and must be 0 in the S-ODT simulations), the only RMS velocity profiles that can be obtained from the model are those shown in Figure 5 (velocity profiles for the streamwise velocity component). $\alpha = 0$ also implies that the kinetic energy is fully contained in the streamwise velocity component, explaining why the RMS profiles for pipe flow ODT simulations lie above the ones for channel flow simulations. For the channel
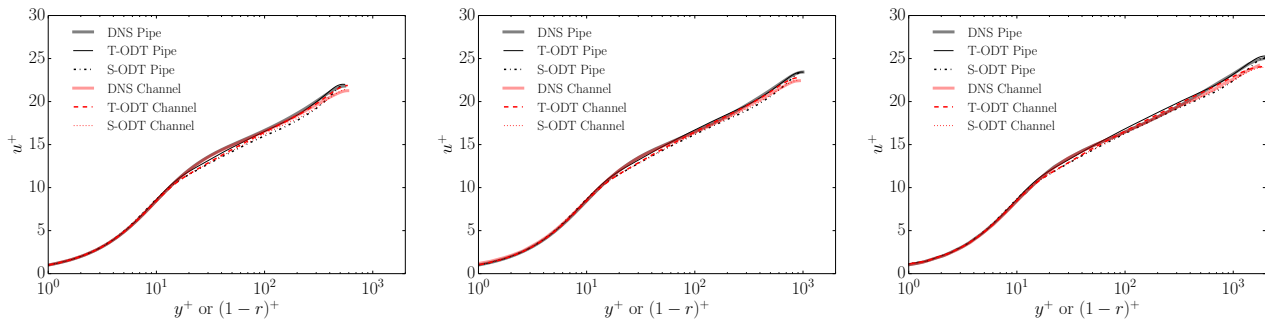
FIGURE 4 Normalized wall-normal mean velocity profiles for ODT channel and pipe flow. a) The low friction Reynolds number case (Case A) is shown along with DNS results from Moser et al.[25] (channel) and Khoury et al.[24] (pipe). b) Case B results are shown along with DNS results from Hoyas and Jiménez[6] (channel) and Khoury et al.[24] (pipe). c) Case C results are shown along with DNS results from Hoyas and Jiménez[6] (channel) and Chin et al.[23] (pipe).

flow case in the T-ODT formulation, we used $\alpha = 2/3$, thus we show also in Figure 5 the results for the u_2 and u_3 (v, w) velocity components in ODT (these results are shown for $Re_\tau = 934$, case B). Both v and w velocity components have the same magnitude in ODT in this case. This is due to the model formulation with $\alpha = 2/3$ and equal initial conditions for both velocity components. These RMS velocity profiles are underpredicted in comparison to DNS data. For channel flow at lower Reynolds numbers, this is consistent with the results of previous ODT publications[17,19].

Figure 6 shows a comparison of the pre-multiplied mean velocity gradient for Case B using the temporal and spatial formulations. In this case, channel DNS results from Jiménez et al.[26] for $Re_\tau = 1000$ and pipe DNS results from Khoury et al.[24] for $Re_\tau = 1000$ were available and used for the comparison. Although the plot dispersion is pronounced in regions far away from the wall, some general trends from the DNS data[23] are confirmed with ODT. In both DNS and ODT, there is no constant region of pre-multiplied velocity gradient beyond the point of departure of the outer buffer layer, which indicates that the logarithmic law does not hold for this case. It is known that such constant profile in the pre-multiplied velocity gradient only starts to appear in fairly large Reynolds numbers regimes[24]. The trends from Case B are also reproduced for Case C in the current simulations without any noticeable difference (not shown here). At least for channel flow, as shown by Lee and Moser[7], the constant profile region for the pre-multiplied velocity gradient starts appearing around $Re_\tau \approx 4200$, a friction Reynolds number which was out of scope for this work. We note that the larger noise component of the plot in regions away from the wall, where a second peak appears between $100 < y^+ < 1000$, is due to the reduced eddy activity in ODT close to the centerline. The infrequent eddy events in this region, thus, require larger averaging periods in order to obtain a fully smooth gradient representation. As noticed in the mean velocity profiles, Figure 4 , we note the larger gradients in the pipe and channel regions close to the centerline in the spatial formulation. We also note a subtle displacement of the first peak of the plot towards the wall, which coincides with the behavior obtained for the RMS velocity profiles.

4.3.2 | TKE Budgets

Following the methodology explained in Section 3, results concerning the calculation of the Reynolds stresses and the TKE budgets are shown next.

Figure 7 shows the Reynolds stress component $\overline{u'v'}$ in the channel and pipe flow simulations with comparison to DNS data. The figure shows that it is possible to achieve a remarkable match between ODT and DNS results, with the best results obtained in the spatial formulation. One point worth stressing is that the calculations done according to Section 3 gathered statistical data only from one side of the domain for the pipe flow case. The reason behind this methodology is that the derivation of the TKE budgets equation was done entirely in differential terms. Thus, a Finite Difference Method (FDM) discretization was used and the origin $r = 0$ had to be avoided. The results for the Reynolds stress show that the ODT model is effectively able to reproduce the energetic interactions in both the channel and pipe-flow simulations. The reader should note that the terminology of the Reynolds stresses used here is the one corresponding to the calculation methods in Section 3.
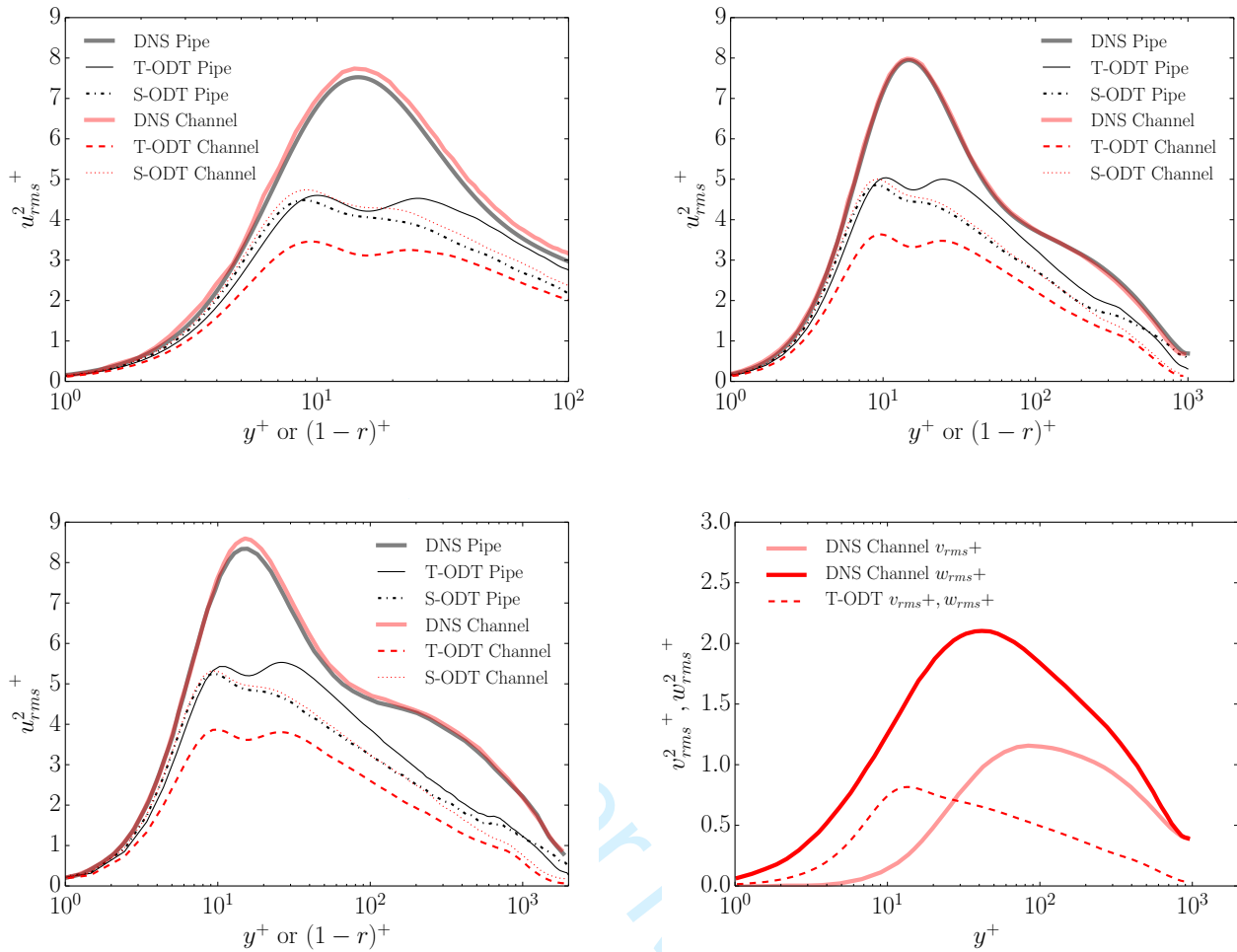
FIGURE 5 Normalized wall-normal RMS velocity profiles for ODT channel and pipe flow. (a): the low friction Reynolds number case (Case A) is shown along with DNS results from Moser et al.[25] (channel) and Khoury et al.[24] (pipe). (b): Case B results are shown along with DNS results from Hoyas and Jiménez[6] (channel) and Khoury et al.[24] (pipe). (c): Case C results are shown along with DNS results from Hoyas and Jiménez[6] (channel) and Chin et al.[23] (pipe). (d): Case B results for channel crosswise and spanwise RMS velocity profiles compared to DNS results from Hoyas and Jiménez[6].

The comparison of the TKE budgets for production and dissipation between the pipe and channel flow simulations is shown in Fig. 8 for Case B. The TKE production is remarkably well reproduced by ODT for both the pipe and channel flow cases. This is not a surprise given the agreement of the Reynolds stresses and the mean velocity profiles shown before. In the case of the TKE dissipation, both ODT results for channel and pipe agree very well with each other, but show some discrepancies with DNS results. The agreement in both ODT cases is also not surprising, given the fact that the TKE dissipation budget solved for the cylindrical formulation is planar, as explained in Section 3. The departure between ODT results and DNS for the TKE dissipation budget can also be partially explained by the overall net TKE magnitude, as seen in the RMS velocity profiles in Figure 5 . In general, the TKE magnitude in ODT is less than that in DNS, which explains why the dissipation budget lies below that of the DNS for large production values[33]. Also, the dissipation budget sink very close to the wall indicates that the dissipation is lower in regions of large production[33]. The latter is a distinct feature of ODT itself, given the instantaneous character of the 1-D eddy events, which are instantaneously created and then subject to diffusive dissipation in the subsequent solution of the moment transport equations. The dissipation budget of the spatial formulation shows increased values between $y^+ \approx 10$ and $y^+ \approx 40$. This region of increased dissipation is in agreement with the region of dissimilar behavior between the temporal and spatial formulation in the streamwise RMS velocity profile. Thus, the increased dissipation in this area is apparently an artifact in the spatial formulation that erodes the second peak in the ODT streamwise turbulence intensity.
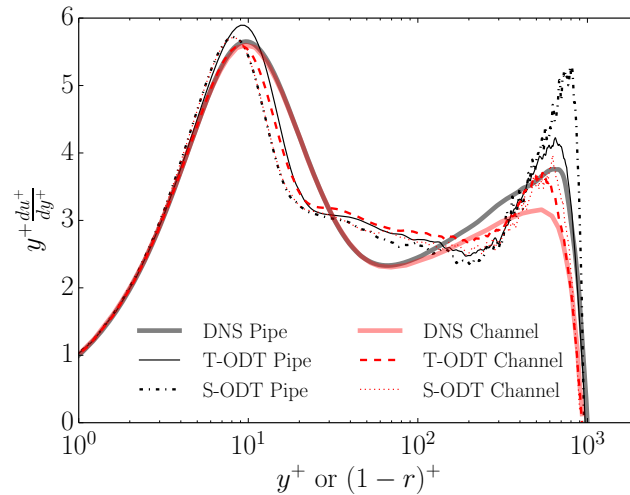
FIGURE 6 Comparison of the pre-multiplied mean velocity gradient for the channel and pipe flow case B simulations. DNS results from Jiménez et al.[26] (channel) and Khoury et al.[24] (pipe) are shown for reference.
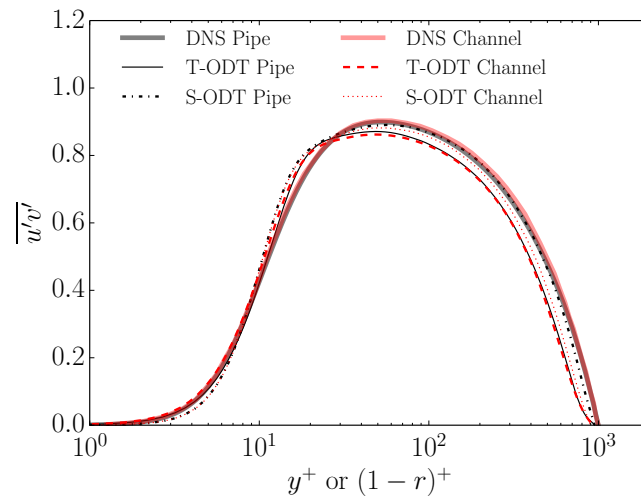
FIGURE 7 Cross-wise Reynolds stress component $\overline{u'v'}$ for Case B simulations. DNS results from Lee and Moser[7] (channel) and Khoury et al.[24] (pipe) are shown along for comparison.

5 | INCOMPRESSIBLE PIPE FLOW RESULTS FOR LOW REYNOLDS NUMBERS

We now present results for an incompressible pipe flow simulation at a lower Reynolds number. This test case is a replication with ODT of the Direct Numerical Simulation (DNS) study by Satake and Kunugi[27]. The test case presents a characteristic low bulk Reynolds number of $Re_b = 5286$, associated with a friction Reynolds number $Re_\tau \approx 180$. Incompressible DNS data at $Re_\tau \approx 180$ taken from Khoury et al.[24] is also used for comparisons in this section.

The T-ODT incompressible formulation uses a time-variable pressure gradient calculation in order to satisfy a constant bulk velocity complying with $Re_b = 5286$. This is done as a one-step correction on the velocity field, once the momentum equation, Eq. (11), has been solved with a zero pressure gradient. The S-ODT incompressible formulation, however, must rely on a constant FPG aimed at obtaining the associated friction Reynolds number $Re_\tau = 180$. In order to obtain the evolution of the passive temperature in the fully developed flow regime, the temporal formulation uses a temperature equation identical to Eq. (12) with the additional advecting term $\int(\rho u c_p \partial \overline{T}/\partial x) r dr$ and constant properties. The mean temperature gradient $\partial \overline{T}/\partial x$ is calculated as in the DNS[27]. As commented in Section 2.2.2, we only perform passive temperature simulations in the T-ODT formulation.
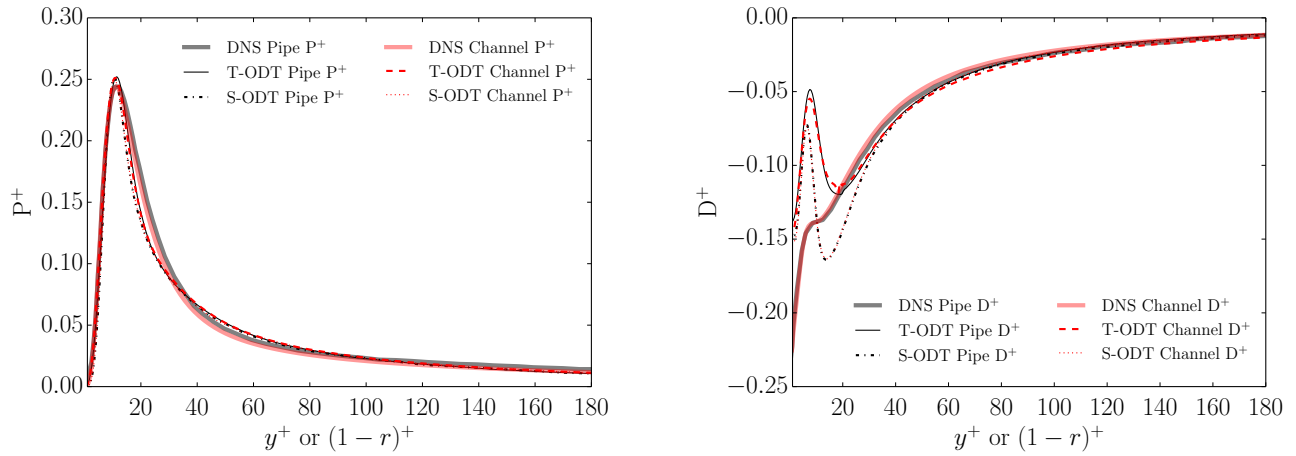
FIGURE 8 TKE Production (P^+) and Dissipation (D^+) budgets for T-ODT and S-ODT simulations (Case B). DNS results from Lee and Moser[7] (channel) and Khoury et al.[24] (pipe) are shown for comparison. (a) Production budget. (b) Dissipation budget.

Trivial initial conditions (uniform profiles) are used for this case. The velocity fields satisfy the no-slip condition at the pipe wall. For the passive scalar T-ODT formulation, the temperature field satisfies an isothermal fixed Dirichlet temperature value at the pipe wall. Table 3 summarises the initial conditions for the test case.

TABLE 3 Parameters used for the low Reynolds number simulations. The diameter of the pipe is indicated by D.

Parameter / Formulation	T-ODT	S-ODT
Target Reynolds number	Bulk $Re_b = 5286$	Friction $Re_\tau = 180$
Momentum Forcing Method	Constant bulk velocity	Fixed Pressure Gradient (FPG)
Momentum Forcing Constant	$U_b = 0.2019$ (m/s)	$\partial \overline{p}/\partial z = -0.0016$ (Pa/m)
Temperature Forcing Method	Fixed Temperature Gradient	N/A
Temperature Forcing Constant	$\partial \overline{T}/\partial z = 1.0661$ (K/m)	N/A
ODT parameter α	0	0
ODT parameter Z	350	100
ODT parameter C	3.5	1.5
Domain Length $D = 2R$ (m)	0.5	
Prandtl Number Pr	0.71 (Air)	
Wall Temperature (T-ODT) T_w (K)	359.802	
Pressure P (Pa)	101350	
Density ρ (kg/m^3)	1.0553	
Kinematic viscosity ν (m^2/s)	1.9105×10^{-5}	
Mesh parameter Δr_C (m)	0.015	
Mesh adaption parameter dxmin $= \eta/6$ (m)	2×10^{-4}	
Mesh adaption parameter dxmax (m)	0.015	
Mesh adaption parameter gDens	80.0	
Mesh adaption parameter DATimeFac	1.3	
Eddy-size PDF L_{max} (normalized by $2R$)	$1/2 = 0.5$	

5.1 | Kinematic statistics

Figure 9 compares the mean velocity profiles obtained with T-ODT at $Re_\tau = 550$ with the ones at $Re_\tau = 180$. We note a severe underestimation of the buffer layer and the logarithmic layer in the T-ODT formulation if the same model parameters from the moderate Reynolds number case are applied in the low Reynolds number case. The most salient feature of these underestimated velocity profiles is the unphysical increase in the mean velocity gradient in the outer layer, close to the centerline region, indicating an excessive local relaminarization. Due to this reason, we adjust the parameter L_{max} in order to account for relative infrequent, yet large eddy events, which may modify the outer layer region. With the less restrictive value of $L_{max} = 1/2$, which was already deemed optimal by Schmidt et al.[19], it is possible to reduce the increase in the outer layer gradients and produce an overall more turbulent outer layer. In Fig. 9 we also show a Cumulative Density Function (CDF) of eddy event sizes for the $Re_\tau = 550$ and $Re_\tau = 180$ cases with model parameters $C = 5$, $Z = 350$ and L_{max} values of $1/3$ and $1/2$. All else being equal, we notice that the CDF of eddy event sizes in Fig. 9 shows an abrupt change of slope for the $Re_\tau = 180$ case with $L_{max} = 1/3$. This implies an abrupt suppression of the eddy size distribution function, and thus, the suppression of important physical phenomena. Effectively, the lower Reynolds number of the flow, or conversely, the laminarization of the flow, provokes that only ever larger eddies are able to induce mixing. We note that the maximum value of L_{max} is 1, which corresponds to an eddy size equal to the length of the domain. Values of L_{max} larger than $1/2$, however, imply for a wall-bounded flow, an eddy larger than the maximum turbulent boundary layer size (half of a channel width, or the pipe radius), which may not be physical. The necessary shift in the velocity profiles to obtain a relatively reasonable match with the DNS results can be achieved afterwards by decreasing the overall turbulence intensity, i.e. lowering the value of the C parameter, as seen also in Figure 9 . Sensitivity to C is expected, given that as C approaches 0, the flow becomes more laminar. Although this sensitivity to the model parameters might seem conflictive with the traditional argumentation in ODT, the reader must recall that, being a turbulence model, ODT is best suited for larger Reynolds numbers flows[34]. Indeed, lowering the model parameter C in the $Re_\tau = 180$ case from $C = 5$ to $C = 3.5$, achieves a better matching with DNS results in the mean profile behavior. The behavior can be optimized by further decrease of the C value. However, this is not done here, since it would affect the prediction of the mean temperature profile (not shown). Therefore, a departure from the outer layer of the flow still takes place in comparison to DNS data: the velocity profiles show a pronounced and steep gradient towards the centerline, and they are still underestimated in the outer buffer layer and in the early regions of the outer layer.

We now compare the selection of model parameters between the incompressible T-ODT and S-ODT formulations. For simplicity and consistency with the T-ODT formulation, we also choose the value $L_{max} = 1/2$ for the spatial formulation. We found a similar sensitivity to the value of C as in the T-ODT formulation. In this case, we must reduce the value of C from $C = 3$ to $C = 1.5$ in order to achieve a reasonable match with DNS results. Figure 10 shows the mean velocity profiles, RMS velocity profiles and transversal $\overline{u'v'}$ Reynolds shear stresses comparing the T-ODT and S-ODT formulations. As expected and due to the temporal and spatial similarity of the fully developed pipe-flow, although the results obtained with both formulations are not identical, the obtained statistics agree reasonably well with each other. With the selected model parameters, the S-ODT mean velocity profile is overestimated in the outer layer region close to the centerline, and it is in general more laminar than its T-ODT counterpart across the outer buffer layer and the entire logarithmic layer. For the Reynolds shear stress $\overline{u'v'}$, there is a reasonable agreement with DNS data in both T-ODT and S-ODT formulations.

Special attention is given to the RMS velocity profiles in Fig. 10 , where the low Reynolds cylindrical formulation produces a triple peak in the T-ODT formulation, which contrasts with the double peak obtained with traditional ODT planar formulations[16] and with the results at larger Reynolds numbers. In comparison, the S-ODT formulation shows also a second peak coinciding with the third peak in T-ODT. This is attributed to the infrequent large scale events which only aid in the reproduction of the ODT mean velocity profile, but which are completely artificial, given that ODT cannot capture or reproduce such large scale behaviour.

5.2 | Passive temperature statistics

Having obtained the optimal parameters for the incompressible kinematic behaviour of the flow at $Re_\tau = 180$, we now examine the results that these parameters produce on the passive temperature behavior using the T-ODT formulation. Figure 11 shows
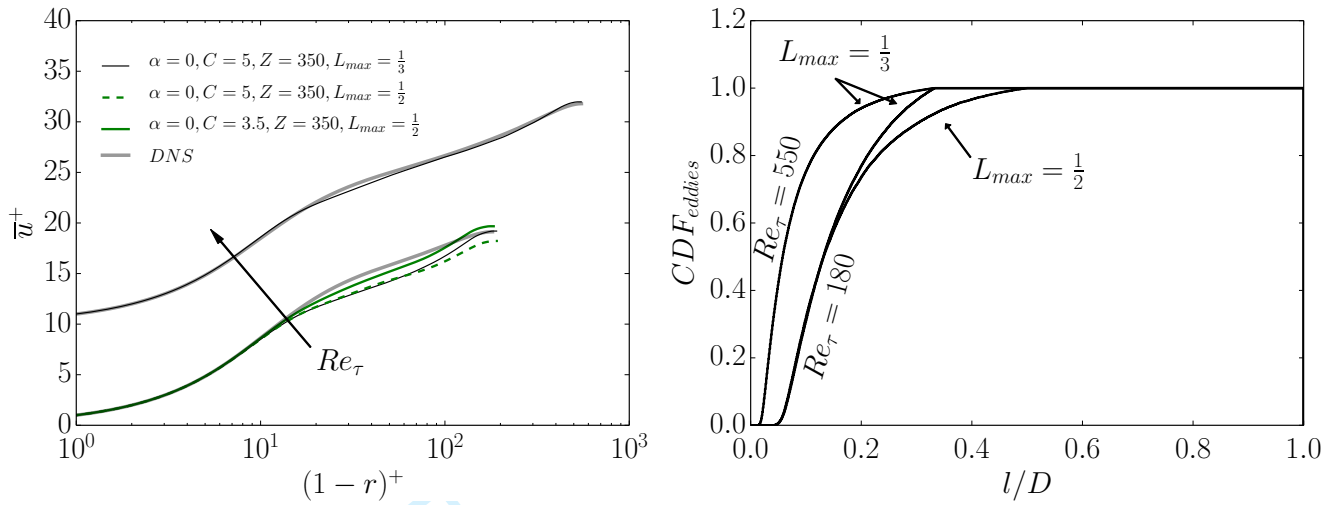
FIGURE 9 Comparison of flow statistics for the T-ODT formulation at $Re_\tau = 180$ and 550. a) Mean velocity profiles at both Reynolds numbers with the effect of the different model parameters C and L_{max}. Profiles at $Re_\tau = 550$ have been shifted by 10 in the vertical axis for better visibility. DNS data[24] is shown for reference. b) CDF of ODT eddy events sizes at equal model parameters $C = 5$, $Z = 350$, $\alpha = 0$ for different values of L_{max}.
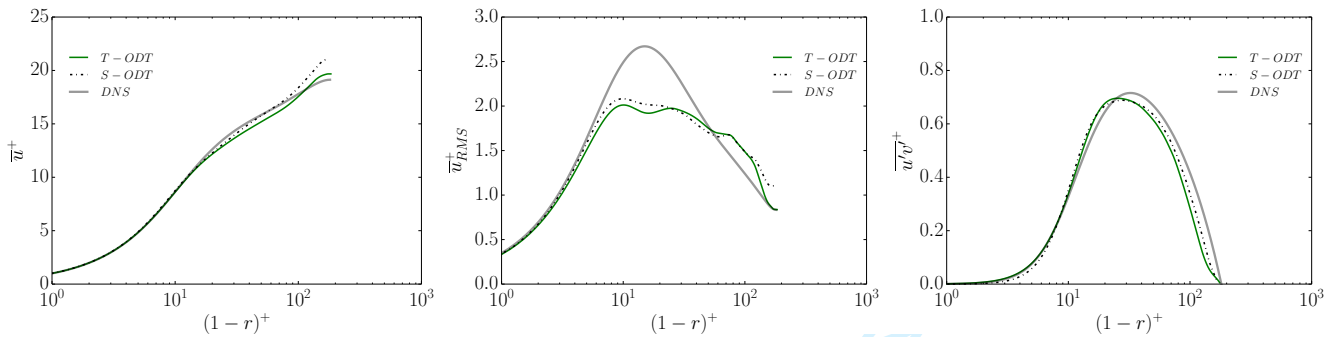
FIGURE 10 Comparison of flow statistics between the T-ODT and S-ODT formulations at $Re_\tau = 180$. a) Mean velocity profiles. b) RMS velocity profiles. c) Transversal $\overline{u'v'}$ Reynolds shear stress. DNS data[24] is shown for reference.

the non-dimensional temperature θ profiles comparing the T-ODT passive temperature results with the DNS data. The non-dimensional temperature θ is defined as,

$$\theta^+ = \frac{T_w - \overline{T}}{T_\tau}, \tag{44}$$

whereby T_w is the fixed wall temperature and T_τ is the friction temperature, as in the DNS[27].

For the non-dimensional temperature profile in Fig. 11, we notice an earlier departure from the DNS data in comparison to the velocity profile in Fig. 10. The temperature solution increases notably in the region surrounding the centerline. Indeed, the temperature profiles obtained with ODT exhibit a much less monotonic behavior in the bulk than the DNS profiles. As in the velocity field, the region where ODT is expected to behave better, close to the wall, achieves a perfect match with DNS. Overall, similarities between the temperature and velocity profiles are expected, not only due to the passive character of the temperature, but also due to the magnitude of the Prandtl number of the flow, which is very close to 1 ($Pr = 0.71$). Aside from the centerline
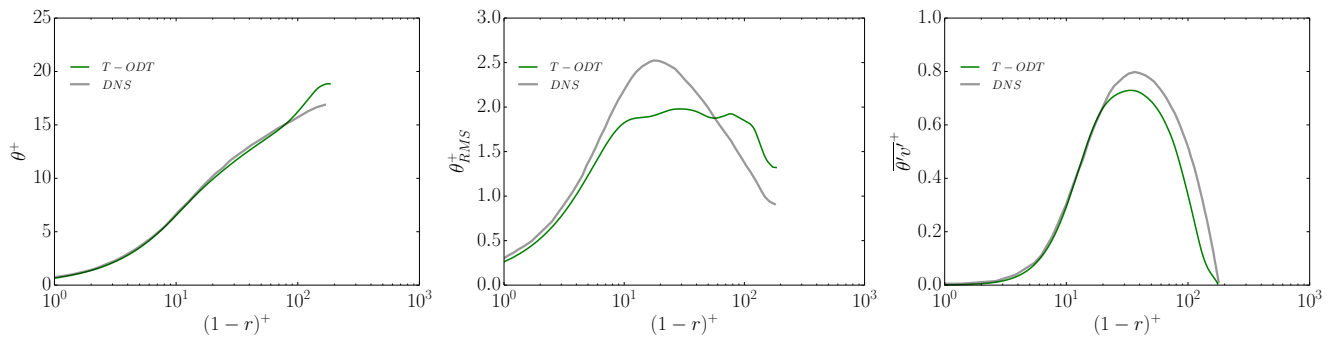
FIGURE 11 Comparison of flow statistics for the T-ODT passive temperature at $Re_b = 5286$. a) Mean non-dimensional temperature profiles. b) RMS non-dimensional temperature profiles. c) Non-dimensional turbulent radial heat flux $\overline{\theta'v'}$. Passive temperature DNS data [27] is used for reference.

anomaly, the behaviour of the ODT results in the outer buffer layer and the early regions of the outer layer is very close to the DNS data. The latter is the reason for our final choice of the T-ODT model parameter $C = 3.5$ in the low Reynolds number case.

The RMS non-dimensional temperature profiles are also shown in Figure 11 . The shallow triple peak seen in the RMS velocity profiles commented in Section 5.1 is seen again in the temperature profiles. Given that the eddy sampling and selection procedure from ODT used in this study is merely based on the available kinetic energy of the flow (and a mechanism for eddy dissipation accounted in a viscous penalty) [28,22], it is not a surprise that the RMS velocity and temperature profiles, which are an indicator of the stationary radial distribution of the streamwise turbulence intensity and turbulent streamwise heat flux, respectively, exhibit the same trend. We do note, however, that the radial distribution of the turbulent streamwise heat flux is much more uniform than its velocity counterpart. This is attributed to the difference in velocity and scalar diffusivities. The larger scalar diffusivity (in comparison to the kinematic viscosity) is able to dissipate scalar fluctuations much faster than the kinematic viscosity dissipates velocity fluctuations across the whole pipe diameter. The behavior of the fully developed turbulent radial heat flux $\overline{\theta'v'}^+$, also shown in Figure 11 is, again, similar to the transversal Reynolds shear stress. Both of these are able to achieve a reasonable match in comparison to the DNS results.

6 | CONCLUSIONS

A detailed study of the cylindrical ODT formulation was carried out in this work. In contrast to the general framework for the cylindrical formulation presented in Lignell et al. [22], an exhaustive analysis of the ODT dynamics for cylindrical pipe flow has been done considering the traditional T-ODT formulation. Additionally, a novel spatial formulation for the channel and pipe flow configurations was introduced, as a demonstrative way to prove the consistency of the temporal and spatial formulations, at least in channel and pipe flows, therefore illustrating the capabilities of the model, while simultaneously presenting new ways to potentially improve results.

Results for the stand-alone ODT model in both its temporal and newly introduced spatial formulations for pipe and channel flows were shown to be able to achieve satisfactory results whenever compared with DNS data. Replicability of the DNS data for the wall-normal mean velocity profiles was obtained for all of the formulations. In general, both the planar and cylindrical ODT formulations are also able to replicate with great accuracy the flow energetics, as shown by the obtained pre-multiplied velocity gradient and cross-wise Reynolds stress behavior.

A calibration process to achieve Reynolds number independent parameters, in the moderate and large Reynolds number range studied here, was successfully carried out. Although it could be argued that the obtained model parameters would be Reynolds number dependent in a range exceeding the one evaluated in this work, it is expected that this sensitivity to the parameters is reduced with the increase of Re_τ and the achievement of an asymptotically turbulent regime [19,22,34]. Having said that, reasonable matches with DNS data were also obtained at the low friction Reynolds number $Re_\tau = 180$. A dependency of the ODT turbulence intensity parameter C was, however, observed with decreasing friction Reynolds number. Although ideally

ODT would be Reynolds number independent (which is effectively true at asymptotically turbulent regimes as commented before), this is consistent with C approaching 0 for laminar flows, i.e. absence of turbulent advection effects.

Despite the solid results shown for the cylindrical formulation in this work, we proved theoretically that the current formulation of the model is only able to reproduce radial fluxes and mimic a planar TKE dissipation term. Although this proved sufficient for this work, it also implies that there is room for improvement in further studies.

Although it was not the main motivation of this work to prove the efficiency of the ODT model against the DNS method, we stress that all of the ODT simulations carried out for this work used, independently, one core of an Intel i7-2600 CPU with 3.4 GHz and 8GByte memory, working in the most severe case (Case C, $Re_\tau = 2003$) with around 2000 grid points due to the adaptive grid implementation. As a reference, the nek5000 pipe flow code used by Khoury et al.[24] required 2.1842×10^9 grid points and employed an available infrastructure of 65,536 cores for the calculation of simulations at $Re_\tau = 1000$. Also, the most expensive channel flow simulation performed in this work, that of $Re_\tau = 2003$, required a computational time with ODT of approximately 160 CPU-h, while, in contrast, the corresponding channel flow simulation of Hoyas and Jiménez[6] required a computational time of 6×10^6 CPU-h. Despite the reduced dimensionality of the model, and therefore its limited applicability range for problems which are homogeneous in at least one direction[14], these details show why the model can be highly appealing for numerical simulations.

ACKNOWLEDGMENTS

Financial disclosure

Conflict of interest

The authors declare no potential conflict of interests.

How cite this article: J. A. Medina Méndez, H. Schmidt, D. O. Lignell, Application of the One-Dimensional Turbulence model to incompressible channel and pipe flow. *Z. Angew. Math. Mech. 2019;00:1–6.*

APPENDIX A CYLINDRICAL TRIPLET MAP

Based on physical reasoning, the cylindrical triplet map formulation is stated for $r \in \mathbb{R}$ instead of the traditional cylindrical treatment of $r \in \mathbb{R}^+$ (non-negative real numbers including 0). This treatment of the cylindrical system allows the occurrence of eddy events involving the centerline, i.e. eddies are allowed to cross the centerline, as in any physical flow.

Since the line integral in a cylindrical system is defined with a differential element $r\mathrm{d}r$, we opt to conserve an effective surface in the cylindrical formulation of the triplet map. The effects of the stochastic eddy events, implemented as triplet maps, which involve wrinkling of the property profiles in the radial direction, can be seen as an assumption that holds for fully developed pipe flows and which is consistent with the 1-D implementation. However, this assumption does not necessarily generalize for other types of cylindrical flows, e.g. in helical flows, where the dominant motion is occuring along the tangential direction. In such cases, modifications of the triplet map and diffusion evolution equations would be necessary. Different formulations for the cylindrical triplet map are also possible, in contrast to the more standardised planar triplet map formulation. Lignell et al.[22]

introduces several formulations for the triplet map, among which the so-called Triplet Map A (TMA) formulation, used here, is the easiest to understand, given its direct analogy to the planar case.

The surface, or volume of the eddy V_{eddy} for the cylindrical formulation, can be expressed as

$$V_{eddy} = \Delta\theta \left[\int_0^{r_0+l} r\mathrm{d}r - \int_0^{r_0} r\mathrm{d}r \right]. \tag{A1}$$

This equation has been formulated considering that $r_0 \geq 0$ for simplicity, and it is equivalent to the volume integral $\Delta\theta \int_{r_0}^{r_0+l} r\mathrm{d}r$.

As in the planar case, the threefold compression of the original profile results in the effective volume of an eddy segment, here denoted as $V_{l/3}$,

$$V_{l/3} = \frac{\Delta\theta}{3} \left[\int_0^{r_0+l} r\mathrm{d}r - \int_0^{r_0} r\mathrm{d}r \right]. \tag{A2}$$

Each segment is defined within two internal boundaries. The position of each of the four boundaries can be expressed with the notation r_m with $m \in \{1,2,3\}$ and $r_0 = r_{m-1}$ for $m = 1$. Each of the three compressed segments accounts then for an effective volume,

$$V_{l/3} = \Delta\theta \left[\int_0^{r_m} r\mathrm{d}r - \int_0^{r_{m-1}} r\mathrm{d}r \right]. \tag{A3}$$

With this notation, the first boundary is r_0 and the last boundary is $r_3 = r_0 + l$. Thus, equating Eq. (A2) with Eq. (A3) and solving for the internal boundary r_m results in,

$$r_m = \left\{ \frac{1}{3} \left[(r_0 + l)^2 - r_0^2 \right] + r_{m-1}^2 \right\}^{\frac{1}{2}}. \tag{A4}$$

Algorithmically, this implies that the calculation of a boundary r_m is done based on the data from the previous boundary r_{m-1}.

We now generalize Eq. (A3) for the case when r_0 is either positive or negative. For that, we make use of the sgn (signum) and modulus functions,

$$V_{l/3} = \Delta\theta \left[\int_0^{|r_m|} r\mathrm{d}r - \mathrm{sgn}(r_m)\,\mathrm{sgn}(r_{m-1}) \int_0^{|r_{m-1}|} r\mathrm{d}r \right]. \tag{A5}$$

In Eq. (A5), the volume can be positive or negative. The latter occurs when r_m and r_{m-1} have both negative sign. A similar procedure can be used to generalize Eq. (A4),

$$|r_m| = \left\{ \frac{1}{3} \left[(r_0 + l)^2 - \mathrm{sgn}(r_0 + l)\,\mathrm{sgn}(r_0)r_0^2 \right] + \mathrm{sgn}(r_m)\,\mathrm{sgn}(r_{m-1})r_{m-1}^2 \right\}^{\frac{1}{2}}. \tag{A6}$$

Eq. (A6) is implicit due to the presence of the $\mathrm{sgn}(r_m)$ term and the LHS modulus. Only one of the two possible solutions is real and within the range $[r_0, r_0 + l]$ in this case.

In order to determine the general expressions for the mapping function of a position $f(r)$ into a new position r, we apply a similar procedure to that used to obtain Eqs. (A2, A5) and (A6). The effective volume of an eddy segment extending from the boundary r_0 to an original position $f(r)$ is conserved and compressed to 1/3 of its magnitude,

$$V_{f(r)} = \frac{\Delta\theta}{3} \left[\int_0^{|f(r)|} r\mathrm{d}r - \mathrm{sgn}[f(r)]\,\mathrm{sgn}(r_0) \int_0^{|r_0|} r\mathrm{d}r \right]. \tag{A7}$$

And conversely, for any mapped position r, that is referenced to the internal boundary r_{m-1}, the effective volume is,

$$V_r = \Delta\theta \left[\int_0^{|r|} r'dr' - \mathrm{sgn}(r)\,\mathrm{sgn}(r_{m-1}) \int_0^{|r_{m-1}|} r'dr' \right]. \tag{A8}$$

Eqs. (A7) and (A8) can be equated, given that any position $f(r)$ will be mapped to a position r within any of the intervals $[r_{m-1}, r_m]$ for $m \in \{1,2,3\}$. This leads to the formal triplet map formulation in a cylindrical coordinate system, as illustrated in Fig. A1 , where the middle segment changes the sign of the slope as in the planar definition,

$$f(r) = \begin{cases} \mathrm{sgn}[f(r)] \left\{ \mathrm{sgn}[f(r)]\,\mathrm{sgn}(r_0)r_0^2 + 3\left[r^2 - \mathrm{sgn}(r)\,\mathrm{sgn}(r_0)r_0^2\right] \right\}^{1/2} & r_0 \leq r \leq r_1, \\ \mathrm{sgn}[f(r)] \left\{ \mathrm{sgn}[f(r)]\,\mathrm{sgn}(r_0)r_0^2 - 3\left[r^2 - \mathrm{sgn}(r)\,\mathrm{sgn}(r_1)r_1^2\right] \right\}^{1/2} & r_1 \leq r \leq r_2, \\ \mathrm{sgn}[f(r)] \left\{ \mathrm{sgn}[f(r)]\,\mathrm{sgn}(r_0)r_0^2 + 3\left[r^2 - \mathrm{sgn}(r)\,\mathrm{sgn}(r_2)r_2^2\right] \right\}^{1/2} & r_2 \leq r \leq r_0 + l. \end{cases} \tag{A9}$$

We note the nonlinear post-triplet map profiles that occur in cylindrical coordinates, as seen in Figure A1 . This is a consequence of the geometric stretching and it is discussed at length in the work of Lignell et al [22].
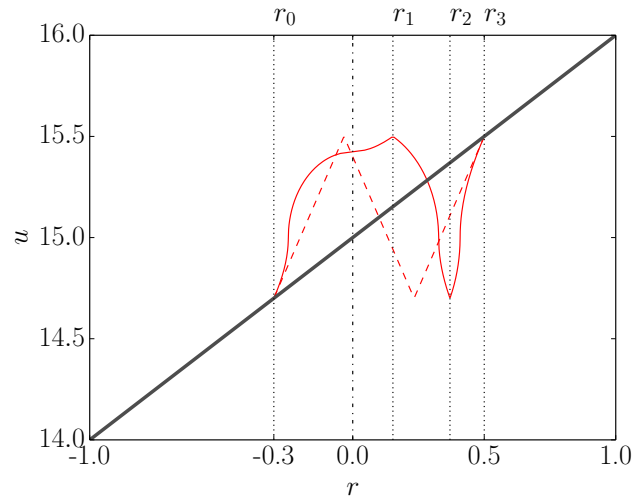
FIGURE A1 Application of a cylindrical triplet map in the range $[-0.3, 0.5]$ to a scalar velocity profile $u(r)$. The figure shows the original profile (thick line) and the mapped profile. The internal boundaries r_m from each of the three segments of the triplet map are also shown (dotted lines), as well as the axis line ($r = 0$) (dash-dot line). For comparison, the planar triplet map for the same interval has been drawn with dashed lines.

APPENDIX B DISCRETIZATION AND NUMERICAL METHOD FOR MOMENTUM DIFFUSION EVOLUTION

B.1 T-ODT formulation

The discretization and numerical advancement of the diffusion evolution PDEs is discussed in this section. The FVM for the integral momentum pipe flow equation, Eq. (11), is obtained by discretization of the r dimension, considering grid cells i with cell interfaces at $i + 1/2$ and $i - 1/2$ (integrals are evaluated within these limits). Constant properties are assumed within cells and the density is a constant. This leads to the discretized equation,

$$\rho \left(\frac{du}{dt} \right)_i (r_i \Delta r_i) = -\frac{\partial \overline{p}}{\partial x} (r_i \Delta r_i) + \left[\left(r_{i+1/2} \mu \frac{u_{i+1} - u_i}{r_{i+1} - r_i} \right) - \left(r_{i-1/2} \mu \frac{u_i - u_{i-1}}{r_i - r_{i-1}} \right) \right]. \tag{B10}$$

We note that $r_i \Delta r_i = [(r_{i+1/2} + r_{i-1/2})/2](r_{i+1/2} - r_{i-1/2}) = (r_{i+1/2}^2 - r_{i-1/2}^2)/2$, which is the same as the result of the integral $\int r dr$ in the cell i, i.e. the radial area/volume of the cell i.

For the case $r_i = 0$, Eq. (B10) contains an apparent singularity if the factor $r_i \Delta r_i$ is rearranged to divide the RHS. The singularity treatment for pipe flow numerical simulations is an old and known problem. In the DNS field, the singularity treatment reduces commonly to one of two approaches: either the discretization is done by effectively suppressing the singularity through the transformation of the cylindrical equations to a polynom-based Spectral Element Method (SEM) (see, e.g. Khoury et al. [24]), or by avoiding the singularity with a special FVM treatment [35]. In this work we have chosen the latter approach. Given that the ODT line mesh is non-uniform, there are three possible choices regarding the cell that contains the position $r = 0$:

- The cell contains the position $r = 0$ at the face (either $r_{i+1/2}$ or $r_{i-1/2}$ are 0).

- The cell is symmetric and contains the position $r_i = 0$ at its center.

- The cell is asymmetric and contains the position $r = 0$.

Examining Eq. (B10) discretized with an explicit method, it should be noted that the 1st option of our list of choices must be discarded, since neglecting either $r_{i+1/2}$ or $r_{i-1/2}$ would effectively neglect the influence of one side of the domain on the other side during the time advancement. This choice is somehow damped, but not entirely removed by choosing the 3rd option of the list. Using the 2nd option in the list with an explicit method supposes another problem, given that the time-derivative is zero due to the factor $r_i \Delta r_i$ when $r_i = 0$. The way then to circumvent this issue is to apply an implicit method along with a symmetric center cell.

If Eq. (B10) is discretized with a backward Euler method solved by means of a Tridiagonal Matrix Algorithm (TDMA), the communication between cells allows the construction of a matrix in which the disappearance of the time derivative factor on the LHS of the equation results in a shear stress flux equalization condition,

$$\left(r_{i+1/2}\mu \frac{u_{i+1} - u_i}{r_{i+1} - r_i} \right) = \left(r_{i-1/2}\mu \frac{u_i - u_{i-1}}{r_i - r_{i-1}} \right). \tag{B11}$$

This expression implies, that within the center cell, there is no net gain or loss of momentum (the incoming fluxes necessarily cancel out the outgoing fluxes). This is similar to the axis averaging methods used by DNS[35]. Also, by solving Eq. (B10) with an implicit method, any discussion regarding the nature of the diffusion CFL condition in cylindrical coordinates is avoided.

The reader is advised at this point that this implicit solution procedure is not exactly the same one done in Lignell et al.[22], where the momentum equation was solved explicitly due to a different treatment of the diffusion in the center cell. In Lignell et al.[22], the center cell term $r_i \Delta r_i = (r_{i+1/2}^2 + r_{i-1/2}^2)/2$, given that $r_{i-1/2}$ and $r_{i+1/2}$ have opposite signs due to the treatment of the coordinate system with $r \in \mathbb{R}$. This is also the result of the integral $\int r dr$ evaluated from 0 to $r_{i+1/2}$ multiplied by 2, which is the factor accounting for an integration over an arc 2π, normalized by π, instead of the standard integration over $\Delta\theta$ for any other disc ring that does not contain the origin. Therefore, in Lignell et al.[22], the singularity is also avoided and an explicit method along with a symmetric center cell is used.

Given that the ODT code used is adaptive, the symmetric center cell implementation encounters a problem that is circumvented by forcing the symmetric center cell with fixed size after every mesh adaption call. This causes strong sensitivity with the mesh adaption, an aspect discussed in Section 4.2. The center cell is considered to have a size equal to dxmax (mesh adaption parameter) in the calibration case $Re_\tau = 590$. Assuming that this center cell is also proportional to the Kolmogorov length scale, we scale the size of the center cell with different friction Reynolds numbers as,

$$\frac{\Delta r_{C,1}}{\Delta r_{C,2}} = \frac{\beta \frac{\nu_1}{u_{\tau,1}}}{\beta \frac{\nu_2}{u_{\tau,2}}} \to \Delta r_{C,2} = \Delta r_{C,1} \frac{Re_{\tau,1}\delta_2}{Re_{\tau,2}\delta_1}. \tag{B12}$$

In Eq. (B12), β is a proportionality constant to relate the center cell size Δr_C with η, where η is the Kolomogorov length scale estimated as ν/u_τ. This consideration is done in order to scale the center cell size as the scaling of the Kolmogorov length scale, although they do not have the same magnitude. u_τ is obtained from the friction Reynolds number definition, which involves δ as the pipe radius.

For the case of T-ODT channel flow, the advancement of the momentum diffusion evolution by Eq. (13) does not require any special treatment. This is carried out in this work by means of a forward Euler explicit method, considering the diffusion CFL condition. The spatial discretization is given by,

$$\rho \left[\frac{du}{dt} \right]_i = -\frac{\partial \overline{p}}{\partial x} + \frac{1}{\Delta y_i} \left[\left(\mu \frac{\partial u}{\partial y} \right)_{i+1/2} - \left(\mu \frac{\partial u}{\partial y} \right)_{i-1/2} \right], \tag{B13}$$

B.2 S-ODT formulation

For the S-ODT pipe flow numerical advancement, some additional considerations in comparison to the temporal formulation must be taken into account. The S-ODT pipe flow case is perhaps the most challenging one in this work, since not only the same considerations of the temporal formulation must be followed (the equation must be solved implicitly), but also due to the presence of the u^2 term that needs to be advanced according to Eq. (17).

In this case, Eq. (17) is discretized implicitly as follows, considering the density as a constant,

$$\rho \frac{u_i^{2,n+1} - u_i^{2,n}}{\Delta x} \left(r_i \Delta r_i \right) = -\frac{\partial \overline{p}}{\partial x} \left(r_i \Delta r_i \right) + \left[\left(r_{i+1/2}\mu \frac{u_{i+1} - u_i}{r_{i+1} - r_i} \right) - \left(r_{i-1/2}\mu \frac{u_i - u_{i-1}}{r_i - r_{i-1}} \right) \right]^{n+1}. \tag{B14}$$

In Eq. (B14), the superindexes n and $n+1$ refer to the spatial positions x_n and x_{n+1}. The backward Euler implicit formulation for the LHS spatial derivative was also used. This equation is solved using the Babylonian method[36], which is a simplification of the general Newton's method. In the Babylonian method, if a is an approximation to $\sqrt{N}$, then the average $1/2(a + N/a)$ is a

better approximation to $\sqrt{N}$. Applying this definition to our discretized Eq. (B14), we compute iteratively the velocity u^{n+1} as,

$$u_i^{n+1} = \frac{1}{2}\left\{ u_i^\star + \frac{u_i^{2,n}\left(r_i\Delta r_i\right) - \frac{\Delta x}{\rho}\frac{\partial \overline{p}}{\partial x}\left(r_i\Delta r_i\right) + \frac{\Delta x}{\rho}\left[\left(r_{i+1/2}\mu\frac{u_{i+1}-u_i}{r_{i+1}-r_i}\right) - \left(r_{i-1/2}\mu\frac{u_i-u_{i-1}}{r_i-r_{i-1}}\right)\right]^{n+1}}{u_i^\star\left(r_i\Delta r_i\right)}\right\}. \tag{B15}$$

Here, a value of $u_i^\star$ is assumed (first guess is $u_i^\star = u_i^n$). A standard implicit TDMA is used to obtain values of u_i^{n+1} with constant value of $u_i^\star$. After this is done, the value of $u_i^\star$ is updated to the value just found for u_i^{n+1}. This procedure is repeated until the residual between two consecutive obtained values of u_i^{n+1} satisfies a given tolerance. We find convergence up to a tolerance approximately equal to 1×10^{-10} m/s determined using a maximum norm in about 5 iterations (as a comparison value for the error tolerance, we consider a reference value of u_τ of 1 m/s).

For the S-ODT channel flow, the advancement is done analogous to the cylindrical formulation, by the formula,

$$u_i^{n+1} = \frac{1}{2}\left\{ u_i^\star + \frac{u_i^{2,n}\left(\Delta y_i\right) - \frac{\Delta x}{\rho}\frac{\partial \overline{p}}{\partial x}\left(\Delta y_i\right) + \frac{\Delta x}{\rho}\left[\left(\mu\frac{u_{i+1}-u_i}{y_{i+1}-y_i}\right) - \left(\mu\frac{u_i-u_{i-1}}{y_i-y_{i-1}}\right)\right]^{n+1}}{u_i^\star\left(\Delta y_i\right)}\right\}. \tag{B16}$$

We note that it would also be possible to advance the planar spatial formulation explicitly as in the temporal formulation, accounting for the advanced quantity u^2 instead of u in Eq. (18). Except for the $\partial/\partial x$ derivative term, the discretization formula for the advancement would be the same as in Eq. (B13). The application of a square root operator should follow after the time-stepping to find the value of u, whereby the positive root should be considered at all times. This is due to the use of the FPG forcing, which, altogether with the assumption of the preservation of the 1-D kinetic energy spectrum ($\alpha = 0$ during an eddy event) guarantees that the velocity field is positive everywhere and at all times.

None of the procedures described here for solving the spatial formulation are the same ones as that used by Lignell et al. [16,22], which is a spatial formulation for open lines. In the before mentioned studies, a non-conservative version of the momentum equation is used, by replacing $\mathrm{d}u^2/\mathrm{d}x$ by $(u)\mathrm{d}u/\mathrm{d}x$ due to the substitution of the continuity equation [22]. As discussed in Section 2.2.2, continuity is a condition which is not solved for closed lines with constant density. Rather, the divergence condition is used.

APPENDIX C CALIBRATION OF THE MODEL PARAMETERS C AND Z FOR THE T-ODT SIMULATIONS

As in any turbulence model, some degree of empiricism is associated with ODT. In our study, this empiricism is related to the determination of the values for the parameters C and Z of the model. On one hand, the C parameter is directly related to the frequency of events being implemented, i.e. the turbulence intensity [28]. On the other hand, the Z parameter is seen as a factor which might effectively deny the implementation of an eddy event. Z is primarily a cutoff mechanism for eddies that, if implemented, might be instantaneously dissipated as heat, thus having essentially no impact in the flow dynamics. Initial values for C and Z for the T-ODT channel and pipe flow simulations were selected based on the evaluations carried out by Lignell et al. [16] and Krishnamoorthy [18] respectively. These values were then subject to a sensitivity study in order to determine the optimal values used in this work (values in Tables 1 and 2).

Figure C2 exemplifies the impact of different C and Z values on T-ODT pipe flow simulations, specifically on the normalized wall normal mean velocity profile. In general, reducing the value of C decreases the number of eddies being implemented and causes a profile behavior closer to the laminar one. Reducing the value of C implies a shift in the logarithmic region towards higher velocity values. This is represented by a moderate increase in the slope of the mean velocity profile in the outer layer.

Traditional evaluations of the Z parameter in ODT identify it as an order unity model parameter [28]. For the case of wall-bounded flows [15,16,18] and recent boundary layer investigations [37], this has been proven as an inadequate generalization. For two-sided wall bounded flows such as the channel and pipe flow configurations evaluated here, the three-dimensional effects of flow structures living in the buffer layer of the flow might be responsible of a significant departure from the ODT model hypothesis. In these cases, Z is instead used in ODT as a tunable cutoff parameter intended to mimic the true behavior of the flow dynamics. In general, increasing the value of Z shifts the logarithmic region of the mean velocity profile upwards, but preserves the slope of the profile. Reducing the value of Z is seen to cause an earlier depature of the velocity profile towards the logarithmic region [37].

Given the tunable nature of the C and Z coefficients, there are different combinations of these parameters that might reproduce different aspects of the flow dynamics. It is possible that a chosen pair of values for C and Z allows good reproducibility of the mean velocity profiles, but not optimal results for the Reynolds stresses [37]. It is also possible that there is more than one pair of values for C and Z that reproduces with reasonable accuracy the true flow dynamics in the mean velocity profile. In the case of this study, we select the optimal values for C and Z based on their effect over the mean velocity profile for the different friction Reynolds numbers given in Tables 1 and 2 . Following the ODT philosophy, the ultimate goal of this calibration process is to achieve a Reynolds number independence of the calibration parameters.
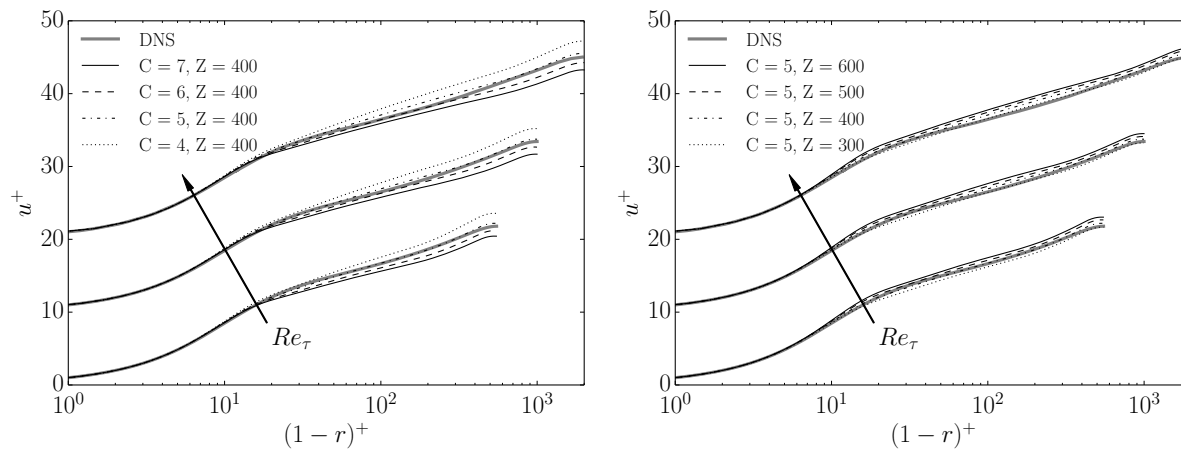
FIGURE C2 Influence of the ODT model parameters on the normalized wall-normal pipe flow mean velocity profile for $Re_\tau = 550, 1000, 2003$. DNS results from Khoury et al. [24] ($Re_\tau = 550, 1000$) and Chin et al. [23] ($Re_\tau = 2003$) are shown for reference. The results for increasing Reynolds numbers have been shifted upwards in the plot for better visualization. a) Influence of C and b) Influence of Z.

APPENDIX D CENTERLINE ANOMALY IN PIPE FLOW RMS VELOCITY PROFILES

During the numerical simulations for pipe flow performed in this work, evidence of anomalous activity around the centerline for the RMS velocity profiles was found for the low Reynolds number case, even when implementing the before discussed center cell treatment. There seems to be a delicate balance of model parameters in pipe flow simulations, which however, can be properly scaled based on all considerations discussed in this paper. We note that this anomaly is also exaggerated due to the use of the Triplet Map A formulation (TMA), in comparison to the TMB formulation used by Lignell et al. [22]. As explained in Lignell et al. [22], in comparison to the TMB formulation, the TMA has a more pronounced spike of the normalized inverse eddy turnover time τ^{-1} in the proximity of $r = 0$. The fact that τ^{-1} first drops at a normalized distance around $2r/l$ and then surges in the proximity to $r = 0$ in TMA, implies that eddies are favored to occur at $r = 0$, but discouraged in the proximity of $r = 0$ up to $2r/l$ [22].

In the mean velocity profiles, this is seen as the relative jump of the profile towards the centerline, where mixing does not take place due to eddies dominantly centered at $r = 0$. Based on this, the dependence on DATimeFac is also justified, given that in order to match the mean velocity profile, we seek a mechanism to introduce more diffusion around the centerline, where the mixing is disproportionate in comparison to the mixing happening right at the center in $r = 0$. This also justifies a dependence on L_{max} for the cylindrical formulation, given that whenever eddies are approximately of size R, the center parcels can be mixed. Influence to L_{max} and DATimeFac was discussed in Section 4.2 from the point of view of the mean velocity profiles, however, the reader can see in Figure D3 , the effect that these parameters have on the RMS velocity profiles. A proper combination of
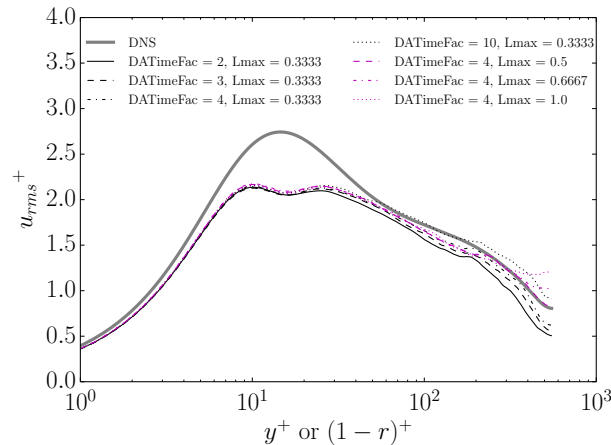
FIGURE D3 Centerline anomaly sensitivity to L_{max} and DATimeFac parameters.

L_{max} and DATimeFac is able to alleviate this centerline anomaly in ODT, which arises due to the characteristics of the cylindrical formulation.

References

[1] I. Marusic, B. J. McKeon, P. A. Monkewitz, H. M. Nagib, A. J. Smits, K. R. Sreenivasan, *Phys. Fluids* **2010** *22*(6), 065103.

[2] X. Wu, P. Moin, *J. Fluid Mech.* **2008**, *608*, 81.

[3] J.P. Monty, J.A. Stewart, R.C. Williams, M.S. Chong, *J. Fluid Mech.* **2007**, *589*, 147.

[4] K. Kim, R. Adrian, *Phys. Fluids* **1999** *11*(2), 417.

[5] J. Ahn, J. H. Lee, J. Lee, J. Kang, H. J. Sung, *Phys. Fluids* **2015** *27*(6), 065110.

[6] S. Hoyas, J. Jiménez, *Phys. Fluids* **2006** *18*(1), 011702.

[7] M. Lee, R. Moser, *J. Fluid Mech.* **2015**, *774*, 395.

[8] M. Hultmark, M. Vallikivi, S. C. C. Bailey, A. J. Smits, *Phys. Rev. Lett.* **2012** *108*(9), 094501.

[9] C. Speziale, *AIAA journal* **1998** *36*(2), 173.

[10] S. Pope, *Turbulent Flows 11th ed.*, Cambridge University Press, **2011**.

[11] J.-L. Wu, H. Xiao, E. Paterson, *Phys. Rev. Fluids* **2018**, *3*, 074602.

[12] M. Ma, J. Lu, G. Tryggvason, *Phys. Fluids* **2015** *27*(9), 092101.

[13] M. Ma, J. Lu, G. Tryggvason, *International Journal of Multiphase Flow* **2016**, *85*, 336 .

[14] A. Kerstein, *J. Fluid Mech.* **1999**, *392*, 277.

[15] F. Meiselbach, Ph.D. thesis, Brandenburgische Technische Universität Cottbus-Senftenberg, **2015**. https://opus4.kobv.de/opus4-btu/frontdoor/index/index/docId/3495.

[16] D. Lignell, A. Kerstein, G. Sun, E. Monson, *Theor. Comput. Fluid Dyn.* **2013** *27*(3-4), 273.

[17] A. Kerstein, W. Ashurst, S. Wunsch, V. Nilsen, *J. Fluid Mech.* **2001**, *447*, 85.

[18] N. Krishnamoorthy, Ph.D. thesis, University of Utah, **2008**.

[19] R. C. Schmidt, A. Kerstein, S. Wunsch, V. Nilsen, *J. Comput. Phys.* **2003**, *186*, 317.

[20] Z. Jozefik, A. Kerstein, H. Schmidt, S. Lyra, H. Kolla, J. Chen, *Combust. Flame* **2015**, *162*, 2999.

[21] J. A. Medina Méndez, H. Schmidt, F. Mauss, Z. Jozefik, *Combust. Flame* **2018**, *190*, 388.

[22] D. O. Lignell, V. B. Lansinger, J. Medina Méndez, M. Klein, A. R. Kerstein, H. Schmidt, M. Fistler, M. Oevermann, *Theor. Comput. Fluid Dyn.* **2018** *32*(4), 495.

[23] C. Chin, J.P. Monty, A. Ooi, *Int. J. Heat Fluid Flow* **2014**, *45*, 33.

[24] G. Khoury, P. Schlatter, A. Noorani, P. Fischer, G. Brethouwer, A. Johansson, *Flow, Turbul. Comb.* **2013**, *91*, 475.

[25] R. Moser, J. Kim, N. Mansour, *Phys. Fluids* **1999** *11*(4), 943.

[26] J. Jimenez, S. Hoyas, M. Simens, Y. Mizuno, *J. Fluid Mech.* **2010**, *657*, 335.

[27] S. Satake, T. Kunugi, *Int. J. Numer. Methods Heat Fluid Flow* **2002** *12*(8), 958.

[28] W. T. Ashurst, A. R. Kerstein, *Phys. Fluids* **2005** *17*(2), 025107.

[29] J. Sutherland, N. Punati, A. Kerstein, A Unified Approach to the Various Formulations of the One-Dimensional-Turbulence Model, *100101*, Institute for Clean and Secure Energy (ICSE), **2010**. https://www.researchgate.net/profile/Alan_Kerstein/publication/266471770_A_Unified_Approach_to_the_Various_Formulations_of_the_One-Dimensional-Turbulence_Model.

[30] Y. Çengel, A. Ghajar, *Heat and Mass Transfer 4th ed.*, McGraw-Hill, **2011**.

[31] A. Shiri, Ph.D. thesis, **2010**. http://www.turbulence-online.com/Publications/Theses/Shiri10.pdf.

[32] M. Klein, H. Schmidt, *Proc. Appl. Math. Mech.* **2017** *17*(17), 639.

[33] F. T. Schulz, C. Glawe, H. Schmidt, A. R. Kerstein, *Environmental Earth Sciences* **2013** *70*(8), 3739.

[34] M. Klein, H. Schmidt, *Proc. Appl. Math. Mech.* **2018** *18*(1), 1.

[35] J. G. M. Eggels, Ph.D. thesis, **1994**. http://resolver.tudelft.nl/uuid:957654af-736a-4923-9490-132538c37062.

[36] D. Fowler, E. Robson, *Historia Mathematica* **1998** *25*(HM982209), 366.

[37] M. M. Fragner, H. Schmidt, *Journal of Turbulence* **2017** *18*(10), 899.